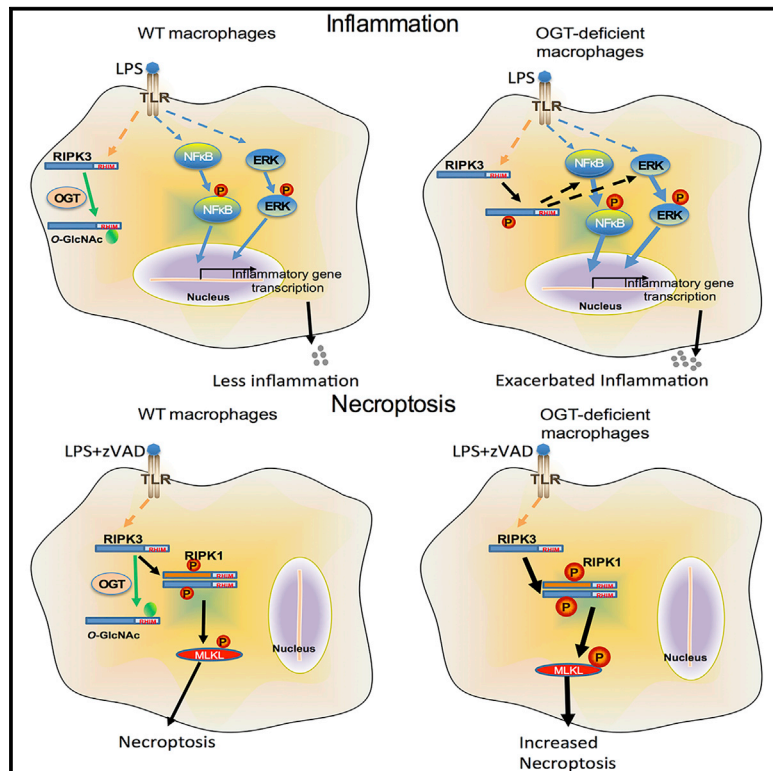


# Immunity

## O-GlcNAc Transferase Suppresses Inflammation and Necroptosis by Targeting Receptor-Interacting Serine/Threonine-Protein Kinase 3

### Graphical Abstract



### Authors

Xinghui Li, Wei Gong, Hao Wang, ..., Douglas R. Green, Pankaj K. Singh, Haitao Wen

### Correspondence

haitao.wen@osumc.edu

### In Brief

The role of individual glucose metabolic pathways in innate immunity remains largely unknown. Li et al. demonstrate that attenuated O-linked  $\beta$ -N-acetylglucosamine (O-GlcNAc) signaling enhances TLR-induced innate immune response and necroptosis. Mechanistically, O-GlcNAcylation of the kinase RIPK3 blocks RHIM-domain-mediated protein interaction and downstream signaling activation.

### Highlights

- LPS treatment causes a decrease in HBP activity and protein O-GlcNAcylation
- OGT deficiency increases activation of innate immune response and necroptosis
- O-GlcNAcylation of RIPK3 on T467 inhibits RIPK3-RIPK1 and RIPK3-RIPK3 interaction



# O-GlcNAc Transferase Suppresses Inflammation and Necroptosis by Targeting Receptor-Interacting Serine/Threonine-Protein Kinase 3

Xinghui Li,<sup>1,13</sup> Wei Gong,<sup>2,13</sup> Hao Wang,<sup>3</sup> Tianliang Li,<sup>1</sup> Kuldeep S. Attri,<sup>4</sup> Robert E. Lewis,<sup>4</sup> Andre C. Kalil,<sup>5</sup> Fatema Bhinderwala,<sup>6</sup> Robert Powers,<sup>6</sup> Guowei Yin,<sup>7</sup> Laura E. Herring,<sup>8</sup> John M. Asara,<sup>9</sup> Yu L. Lei,<sup>10</sup> Xiaoyong Yang,<sup>11</sup> Diego A. Rodriguez,<sup>12</sup> Mao Yang,<sup>12</sup> Douglas R. Green,<sup>12</sup> Pankaj K. Singh,<sup>4</sup> and Haitao Wen<sup>1,14,\*</sup>

<sup>1</sup>Department of Microbial Infection and Immunity, Infectious Disease Institute, The Ohio State University Comprehensive Cancer Center, The Ohio State University, Columbus, OH 43210, USA

<sup>2</sup>Department of Hepatobiliary Surgery and Liver Transplantation, Shandong Provincial Hospital Affiliated to Shandong University, Jinan, Shandong, China

<sup>3</sup>Department of Critical Care Medicine, Qilu Hospital of Shandong University, Jinan, Shandong, China

<sup>4</sup>Eppley Institute for Research in Cancer and Allied Diseases, Nebraska Medical Center, Omaha, NE 68198, USA

<sup>5</sup>Department of Internal Medicine, Division of infectious Diseases, University of Nebraska Medical Center, Omaha, NE 68198, USA

<sup>6</sup>Department of Chemistry, Nebraska Center for Integrated Biomolecular Communication, University of Nebraska-Lincoln, Lincoln, NE 68588, USA

<sup>7</sup>Department of Psychiatry, Vagelos College of Physicians and Surgeons, Columbia University, New York, NY 10032, USA

<sup>8</sup>Proteomics Core Facility, Department of Pharmacology, University of North Carolina at Chapel Hill, Chapel Hill, NC 27599, USA

<sup>9</sup>Division of Signal Transduction, Beth Israel Deaconess Medical Center and Department of Medicine, Harvard Medical School, Boston, MA 02215, USA

<sup>10</sup>Department of Periodontics and Oral Medicine, University of Michigan School of Dentistry, University of Michigan Rogel Cancer Center, University of Michigan, Ann Arbor, MI 48105, USA

<sup>11</sup>Program in Integrative Cell Signaling and Neurobiology of Metabolism, Department of Comparative Medicine, Yale University School of Medicine, New Haven, CT 06520, USA

<sup>12</sup>Department of Immunology, St. Jude Children's Research Hospital, Memphis, TN 38105, USA

<sup>13</sup>These authors contributed equally

<sup>14</sup>Lead Contact

\*Correspondence: [haitao.wen@osumc.edu](mailto:haitao.wen@osumc.edu)

<https://doi.org/10.1016/j.immuni.2019.01.007>

## SUMMARY

Elevated glucose metabolism in immune cells represents a hallmark feature of many inflammatory diseases, such as sepsis. However, the role of individual glucose metabolic pathways during immune cell activation and inflammation remains incompletely understood. Here, we demonstrate a previously unrecognized anti-inflammatory function of the O-linked  $\beta$ -N-acetylglucosamine (O-GlcNAc) signaling associated with the hexosamine biosynthesis pathway (HBP). Despite elevated activities of glycolysis and the pentose phosphate pathway, activation of macrophages with lipopolysaccharide (LPS) resulted in attenuated HBP activity and protein O-GlcNAcylation. Deletion of O-GlcNAc transferase (OGT), a key enzyme for protein O-GlcNAcylation, led to enhanced innate immune activation and exacerbated septic inflammation. Mechanistically, OGT-mediated O-GlcNAcylation of the serine-threonine kinase RIPK3 on threonine 467 (T467) prevented RIPK3-RIPK1 hetero- and RIPK3-RIPK3 homo-interaction and inhibited downstream innate immunity and necroptosis signaling. Thus, our study identifies an immuno-metabolic crosstalk essential for fine-

tuning innate immune cell activation and highlights the importance of glucose metabolism in septic inflammation.

## INTRODUCTION

Reprogramming of cellular metabolic activities has recently been demonstrated to play a critical role in the activation of the immune system and hyperinflammation (Buck et al., 2017; O'Neill et al., 2016). Increased glucose uptake and glycolysis occur in classically activated innate immune cells *in vitro* and *in vivo* (Everts et al., 2014). A widely accepted concept in the immunometabolism research field is that elevated catabolic activity in activated immune cells is necessary for meeting the increased demand of biomolecules and energy for effective immune functions. Those functions (including cell migration, phagocytosis, and cytokine production) are necessary for host response against invading pathogens or tissue injury during inflammation. Recent progress has broadened our understanding of how metabolic reprogramming modulates immune functions in multiple aspects. For example, a variety of metabolic enzymes involved in the glycolysis and mitochondrial metabolic pathways have been identified as playing essential roles in affecting innate immune cell function (O'Neill et al., 2016). Moreover, many intermediate metabolites, such as succinate (Tannahill et al., 2013), fumarate (Arts et al., 2016), itaconate (Bambouskova et al., 2018; Mills et al., 2018),



and  $\alpha$ -ketoglutarate (Liu et al., 2017), have recently been reported to participate in immune activation or modulation. Therefore, the metabolic system regulates immune cell function and inflammation through combined strategies.

Glucose serves as a major nutrient to fuel cellular metabolic activities. Three major glucose metabolic pathways, namely glycolysis, the pentose phosphate pathway (PPP), and the hexosamine biosynthesis pathway (HBP), collaboratively determine how glucose is processed. HBP is a unique glucose metabolism pathway leading to the generation of its end product uridine diphosphate *N*-acetylglucosamine (UDP-GlcNAc), which is further utilized by the *O*-GlcNAc transferase (OGT) for protein modification, namely *O*-GlcNAcylation (Levine and Walker, 2016). Many proteins involved in various fundamental biological processes, including transcription factors, kinases, and enzymes, have been identified as *O*-GlcNAcylation targets (Yang and Qian, 2017). Recent studies have identified several molecules involved in the innate immune signaling as *O*-GlcNAcylation targets. For example, *O*-GlcNAcylation of IKK $\beta$ , NF- $\kappa$ B p65, c-Rel, and TAB1 enhances their activities and promotes the transcription of NF- $\kappa$ B target genes. (Ozcan et al., 2010; Pathak et al., 2012; Yang et al., 2015c). We recently identified *O*-GlcNAcylation of the transcription factor STAT3 as an important mechanism antagonizing its activation (Li et al., 2017). However, the specific role of OGT in innate immune function and inflammation remains poorly defined.

RIPK3 is a member of the receptor-interacting protein (RIP) family of serine/threonine kinases and contains an N-terminal kinase domain and a C-terminal RIP homotypic interaction motif (RHIM) (Silke et al., 2015). Through RHIM-mediated protein interaction, RIPK3 forms a necrosome complex with RIPK1, and this complex is required for the induction of necroptosis, an inflammatory form of cell death (Galluzzi et al., 2017; Weinlich et al., 2017). Both RHIM and kinase activity of RIPK3 are essential for activation of downstream effector protein MLKL and execution of necroptosis (Wallach et al., 2016). In addition to having a central role in necroptosis, elevated RIPK3 activation has been shown to promote inflammatory responses in both cell-death-dependent and -independent manners (Alvarez-Diaz et al., 2016; Moriwaki et al., 2017; Najjar et al., 2016). Despite being a well-studied signaling pathway leading to necrosome formation, the intrinsic mechanism modulating RIPK3 activation is not well understood. In this study, we identified OGT-mediated RIPK3 *O*-GlcNAcylation at T467 as a key mechanism to block RHIM-mediated RIPK3-RIPK1 and RIPK3-RIPK3 interaction. Removal of OGT or RIPK3 *O*-GlcNAcylation promoted macrophage inflammatory response and necroptosis, both of which are dependent on RIPK3 RHIM domain and kinase activity. As a result, genetic deletion of *Ogt* in myeloid cells markedly exacerbated cytokine storm and host mortality in experimental sepsis. Therefore, our findings demonstrate a check mechanism against overzealous innate immune activation through OGT-mediated RIPK3 *O*-GlcNAcylation.

## RESULTS

### Lipopolysaccharide Attenuates HBP Activity and Protein *O*-GlcNAcylation in Macrophages

Increased glucose uptake and glycolysis have been well documented in activated immune cells (Everts et al., 2014).

We compared intracellular metabolite profiles between mock-treated and LPS-stimulated mouse bone-marrow-derived macrophages (BMMs) by performing metabolomics analyses. Principal-component analysis revealed a markedly altered metabolic profile upon LPS stimulation (Figure 1A). Pathway-enrichment analysis identified several sugar-related metabolic pathways (fructose and mannose, pyruvate, and glycolysis) among the most differentially regulated pathways (Figures 1B and 1C). Many intermediate metabolites involved in glycolysis (Figure 1D) and the PPP (Figure 1E) showed increased abundance upon LPS challenge (Table S1). Several HBP metabolites were decreased after LPS stimulation, including HBP end product UDP-GlcNAc (Figures 1F and S1). Metabolic tracer analysis using  $^{13}$ C-glucose tracing also revealed an increased incorporation of glucose-derived carbon in glycolysis (Figure 1G) and decreased incorporation into HBP metabolites (Figure 1H and Table S2), which suggests that LPS attenuated HBP activity.

The availability of UDP-GlcNAc is an important determinant of OGT enzymatic activity (Hart et al., 2011). Consistent with decreased UDP-GlcNAc abundance, LPS-stimulated BMMs exhibited attenuated total protein *O*-GlcNAcylation without affecting the amount of OGT (Figure 1I). In an experimental sepsis model induced by the cecal ligation and puncture (CLP) procedure (Wen et al., 2010), peritoneal macrophages isolated from septic mice 24 h after CLP exhibited markedly attenuated protein *O*-GlcNAcylation compared with that in sham mice (Figure 1J). The *O*-GlcNAc signal was abolished when anti-*O*-GlcNAc antibody was pre-incubated with 500 mM *N*-acetylglucosamine (GlcNAc), indicating the specificity of *O*-GlcNAc signal. These findings demonstrate that classical activation of macrophages leads to attenuated HBP activity and protein *O*-GlcNAcylation *in vitro* and *in vivo*.

### OGT Inhibits Activation of the Innate Immune Response

We examined the function of OGT-mediated *O*-GlcNAc signaling in the activation of the innate immune responses. Upon LPS challenge, *Ogt*<sup>fl/fl</sup>*xLyz2-cre* BMMs (Li et al., 2018) produced significantly higher amounts of inflammatory mediators at transcript (Figure 2A) and protein (interleukin-6 [IL-6] and tumor necrosis factor  $\alpha$  [TNF- $\alpha$ ]) (Figure 2B) concentrations than did *Ogt*<sup>fl/fl</sup> BMMs. Induction of Nos2 and nitrite production by LPS was also enhanced in *Ogt*<sup>fl/fl</sup>*xLyz2-cre* BMMs (Figures 2C and 2D). Treatment with Toll-like receptor 2 (TLR2) (Pam3Cys) or TLR9 (CpG) agonists showed similar phenotypes (Figures 2E and 2F). M2-associated gene transcripts (Figure S2A) and arginase-1 protein (Figure S2B) were normally induced in IL-4-treated *Ogt*<sup>fl/fl</sup>*xLyz2-cre* BMMs, indicating no defect in *Ogt*<sup>fl/fl</sup>*xLyz2-cre* BMM M2 polarization. Furthermore, OGT-deficient human monocyte-like THP-1 cells (Li et al., 2018) produced significantly higher amounts of inflammatory cytokines in response to TLR2, TLR4, or TLR9 agonist than did control THP-1 cells, suggesting that OGT negatively regulates cytokine production both in mouse and in human cells (Figure S2C).

We have recently reported that OGT-mediated STAT3 *O*-GlcNAcylation antagonizes STAT3 phosphorylation and IL-10 production (Li et al., 2017). Further assays with the use of *Ogt*<sup>fl/fl</sup>*xLyz2-cre* macrophages revealed that *Ogt* deletion indeed resulted in enhanced Stat3 phosphorylation (Figure S3A) and IL-10 production (Figures S3B and S3C) upon TLR activation.

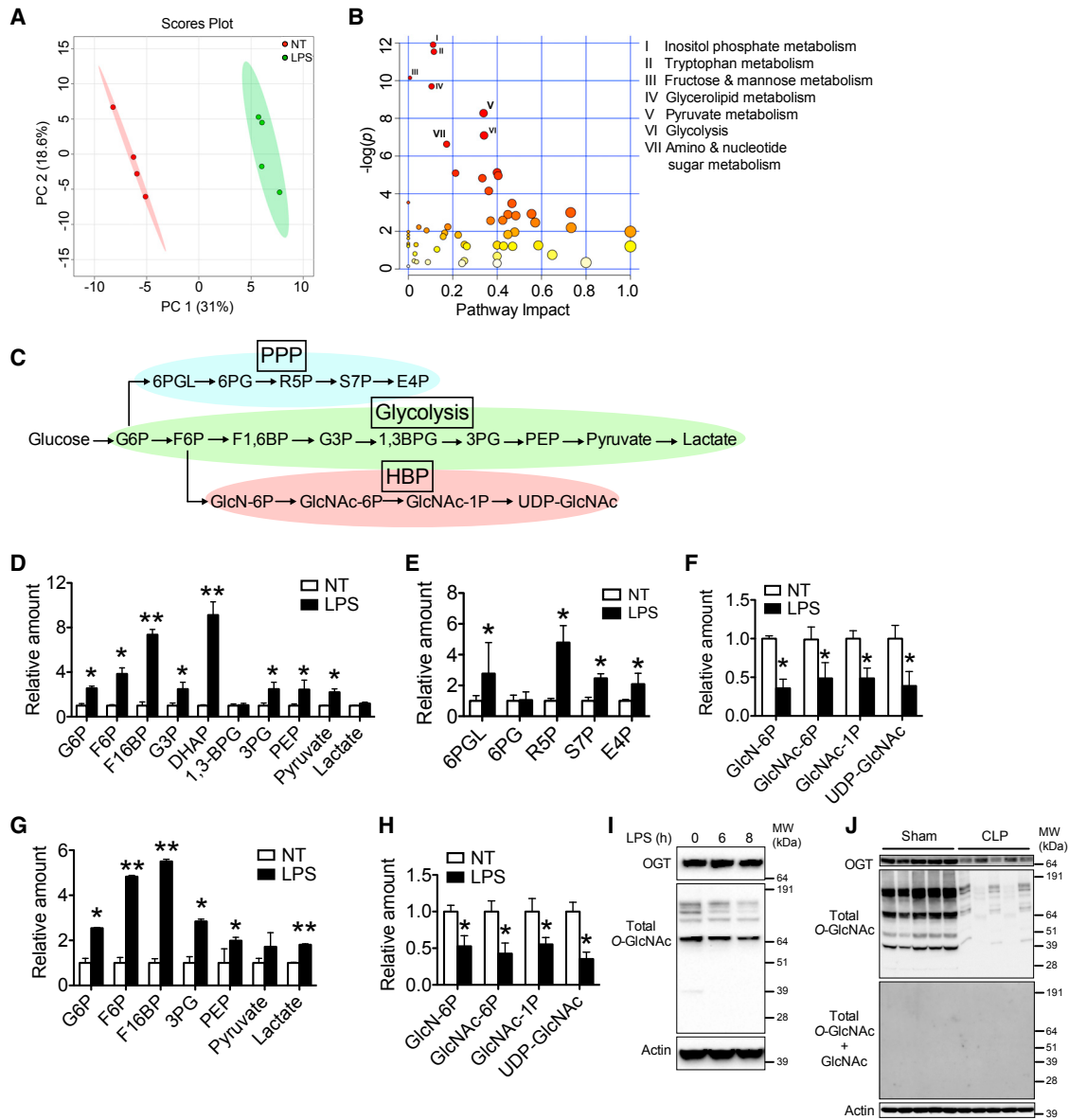


**Figure 1. LPS Stimulation Affects Glucose Metabolism in Mouse Macrophages**

(A and B) Total metabolite profiling in mouse BMMs stimulated with or without LPS (200 ng/mL) for 6 h was determined by the metabolomics assay based on liquid chromatography-tandem mass spectrometry (LC-MS/MS) and assessed by principle-component analysis (A) and pathway-enrichment analysis (B).

(C) A schematic of three glucose metabolic pathways: glycolysis (middle), PPP (upper), and HBP (lower).

(D–F) LPS-induced fold changes in intermediate metabolites of glycolysis (D), PPP (E), and HBP (F) in mouse BMMs.

(G and H) LPS-induced fold changes in <sup>13</sup>C-intermediate metabolites of glycolysis (G) and HBP (H) in mouse BMMs in the presence of <sup>13</sup>C<sub>6</sub>-glucose.

(I and J) Immunoblotting of OGT and total O-GlcNAc in mouse BMMs (I) or peritoneal macrophages isolated from mice 24 h after a sham or cecal ligation and puncture (CLP) procedure (J).

\*p < 0.05, \*\*p < 0.01 versus controls (two-tailed Student's t test in E–H). Data are from one experiment representative of three experiments (A, B, D–F; mean ± SD of four biological replicates) or two experiments (G and H; mean ± SD of three biological replicates) or four experiments (I and J). Please also see Figure S1.

Pretreatment of cells with the specific Stat3 inhibitor S31-201 (Siddiquee et al., 2007) completely abolished the increased IL-10 production in *Ogt<sup>fl/fl</sup>xLyz2-cre* macrophages; however, increased IL-6 and TNF- $\alpha$  production was still maintained in *Ogt<sup>fl/fl</sup>xLyz2-cre* macrophages (Figure S3D). These results indicate that the hyperinflammatory response in *Ogt<sup>fl/fl</sup>xLyz2-cre* macrophages is caused by a Stat3-independent mechanism.

Activation of innate immune signaling, such as the NF- $\kappa$ B and MAPK pathways, is essential for TLR-induced cytokine production. We observed increased activation of the NF- $\kappa$ B pathway as evidenced by phosphorylation of IKK $\alpha$ / $\beta$ , I $\kappa$ B $\alpha$ , and p65 in LPS-challenged *Ogt<sup>fl/fl</sup>xLyz2-cre* BMMs (Figure 2G), as well as enhanced phosphorylation of Erk, but not p38 or Jnk (Figure 2H). Furthermore, by isolating macrophage cytosolic and nuclear

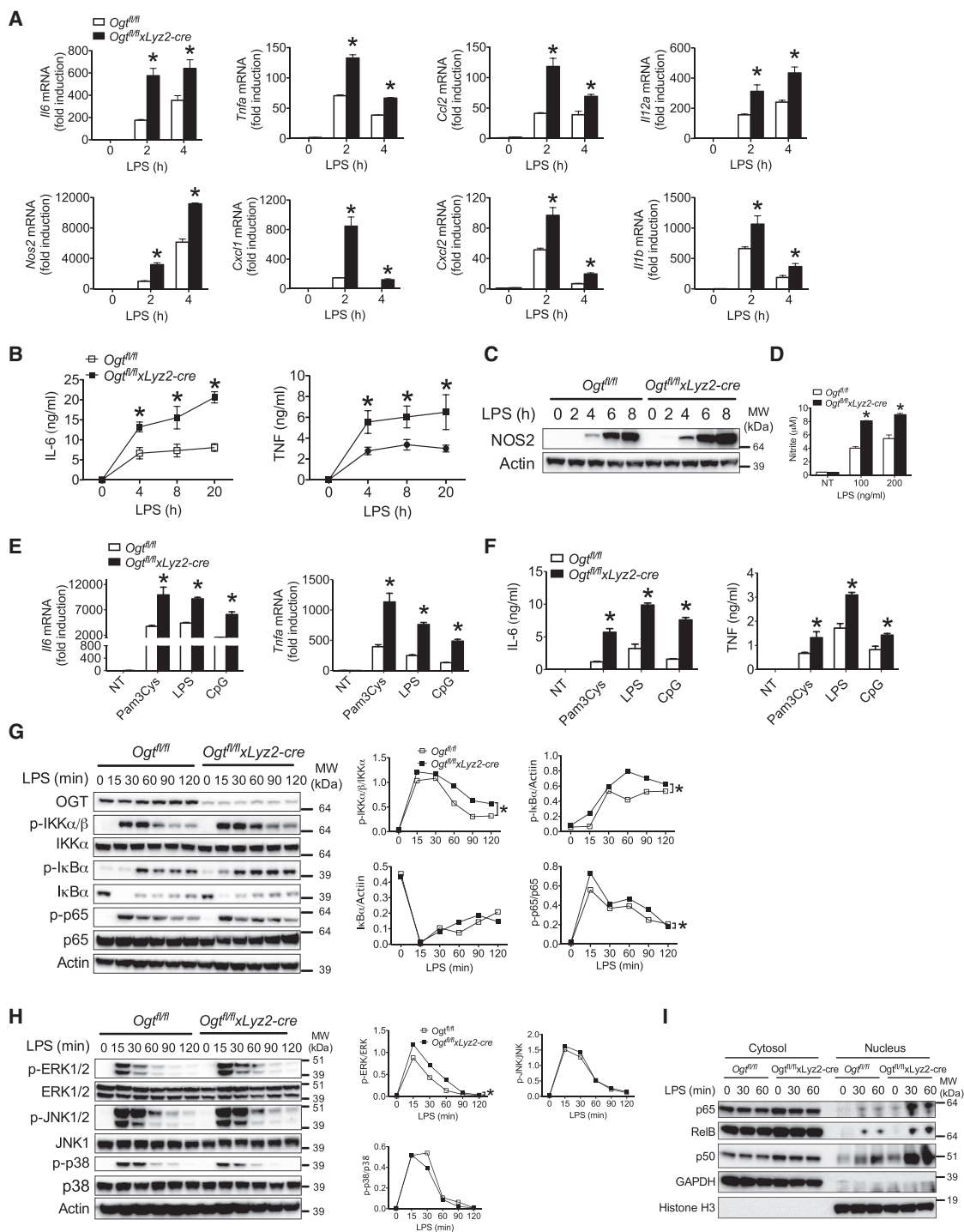


### Figure 2. OGT Deficiency Enhances Activation of the Innate Immune Responses

(A–F) BMMs generated from *Ogt<sup>fl/fl</sup>* and *Ogt<sup>fl/fl</sup>xLyz2-cre* mice were left untreated or were stimulated with LPS (A–D and G–I) or Pam3Cys or CpG (E and F) for the indicated periods. Transcripts of inflammatory genes (A and E), IL-6 and TNF- $\alpha$  (B and F), and nitrite concentrations (D) in the supernatants were measured with RT-PCR, ELISA, and the Griess assay, respectively. Nos2 was assayed by immunoblotting (C).

(G and H) Immunoblotting of NF- $\kappa$ B (G, left) and MAPK (H, left) signaling molecules and densitometric analysis (G and H, right).

(I) Immunoblotting of NF- $\kappa$ B p65, RelB, and p50 in the cytosolic (left) and nuclear (right) compartments.

\* $p < 0.05$  versus controls (two-tailed Student's *t* test). Data are from one experiment representative of five experiments (A, B, and D–F; mean  $\pm$  SD of four biological replicates) or four experiments (C, G, H, and I). Please also see Figure S2 and S3.

compartments, we found markedly increased nuclear translocation of p65, RelB, and p50 in LPS-stimulated *Ogt<sup>fl/fl</sup>xLyz2-cre* BMMs, lending further support to increased NF- $\kappa$ B activation (Figure 2I). In sum, these findings collectively demonstrate that OGT deficiency leads to the hyperactivation of TLR-mediated innate immune signaling.

### Myeloid *Ogt* Deletion Exacerbates Septic Inflammation

To examine the function of myeloid-derived OGT in the innate immune response *in vivo*, we employed two septic inflammation models: endotoxin shock induced by intraperitoneal LPS injection and CLP-induced polymicrobial peritonitis (Wen et al., 2010). After administration of LPS at 15 mg per kg body weight, 60% of wild-type (WT) mice survived within 48 h, whereas all *Ogt<sup>fl/fl</sup>xLyz2-cre* mice died over the same period (Figure 3A). Analyses of inflammatory cytokines in the peritoneal lavage fluid or serum revealed an exacerbated cytokine storm in *Ogt<sup>fl/fl</sup>xLyz2-cre* mice (Figures 3B and 3C). During a mild experimental sepsis model induced by a two-puncture CLP procedure, *Ogt<sup>fl/fl</sup>xLyz2-cre* mice were significantly susceptible to CLP-induced lethality in sepsis (Figure 3D), accompanied by significantly elevated inflammatory cytokine production in the peritoneal lavage fluid (Figure 3E), serum (Figure 3F), and lung homogenate (Figure 3G). Therefore, OGT in myeloid cells is crucial to limiting hyperactivation of the innate immune response and protects hosts from sepsis-induced lethality. It is well known that sepsis causes massive T cell apoptosis, which plays an important role in promoting immunosuppression following sepsis (Hotchkiss et al., 2013). However, we found no significant difference in T-cell-associated cytokines IL-2 and IFN- $\gamma$  in serum (Figure S4A) or the numbers of CD3<sup>+</sup>CD4<sup>+</sup> or CD3<sup>+</sup>CD8<sup>+</sup> T cells in the spleen (Figure S4B) or inguinal lymph nodes (Figure S4C) between septic WT and *Ogt<sup>fl/fl</sup>xLyz2-cre* mice. Therefore, increased mortality in septic *Ogt<sup>fl/fl</sup>xLyz2-cre* mice is not likely to be due to altered T cell responses.

### Deletion of *Ripk3* Abolishes Hyperinflammation in *Ogt<sup>fl/fl</sup>xLyz2-cre* Macrophages and in Mice

We next sought to determine at which level OGT inhibits TLR-induced innate immune signaling by performing a NF- $\kappa$ B-driven luciferase assay. OGT inhibited NF- $\kappa$ B-dependent luciferase gene transcription induced by MYD88, TRAF6, RIPK1, and RIPK3 but showed no inhibitory effect on IKK1-, IKK2-, or p65-driven NF- $\kappa$ B activation (Figure 4A). These results suggest that OGT is functioning at the RIPK1 and/or RIPK3 level. Nec-1 (Degterev et al., 2008) and GSK-872 (Mandal et al., 2014) are well-defined kinase activity inhibitors for RIPK1 and RIPK3, respectively. Treatment with GSK-872, but not Nec-1, abolished increased cytokine production in *Ogt<sup>fl/fl</sup>xLyz2-cre* BMMs (Figures S5A and S5B), as well as in OGT-deficient THP-1 cells (Figure S5C). We next tested BMMs generated from *Ripk1<sup>K45A</sup>*- (Berger et al., 2014) or *Ripk3<sup>K51A</sup>*- (Mandal et al., 2014) kinase dead mice. Pharmacological inhibition of OGT by OSMI-1 (Li et al., 2018) promoted LPS-induced cytokine production in WT BMMs to the same concentrations as those in *Ogt<sup>fl/fl</sup>xLyz2-cre* BMMs, indicating that OSMI-1 treatment caused an OGT-dependent hyperinflammatory response (Figures S5D and S5E). Importantly, OSMI-1 treatment selectively increased LPS-induced cytokine production in *Ripk1<sup>K45A</sup>* BMMs, but not

in *Ripk3<sup>K51A</sup>* BMMs (Figures S5F and S5G). Together, these findings suggest that the kinase activity of RIPK3, but not RIPK1, is required for increased cytokine production in LPS-treated *Ogt<sup>fl/fl</sup>xLyz2-cre* BMMs.

It has been well established that genetic deletion of apoptosis-associated effector molecules, such as caspase-8, promotes RIPK3-dependent necroptotic and inflammatory responses (Galluzzi et al., 2017; Weinlich et al., 2017). We found that, compared with WT BMMs, *Ogt<sup>fl/fl</sup>xLyz2-cre* BMMs generated higher amounts of both IL-1 $\beta$  and IL-6 in response to the agonists of either canonical (LPS plus ATP, nigericin, silica, or alum) (Figure S5H) or noncanonical (LPS plus cholera toxin B [CTB]) inflammasomes (Figure S5I). Given that LPS stimulation alone caused no IL-1 $\beta$  release in *Ogt<sup>fl/fl</sup>xLyz2-cre* BMMs, we concluded that OGT deficiency enhances the “priming” phase, as evidenced by increased *I1b* transcription (Figure 2A), but not the “activating” phase of inflammasome activation. Furthermore, we found no difference in caspase-8 amounts between WT and *Ogt<sup>fl/fl</sup>xLyz2-cre* BMMs (Figures S5J and S5K) and detected no O-GlcNAc signal on exogenously expressed caspase-8 (Figure S5L). Therefore, it seems not likely that OGT affects RIPK3 activity through caspase-8.

We generated *Ogt<sup>fl/fl</sup>xLyz2-creRipk3<sup>-/-</sup>* mice to test whether additional deletion of *Ripk3* could reverse the hyperinflammatory phenotype in *Ogt<sup>fl/fl</sup>xLyz2-cre* macrophages and mice. Compared with *Ogt<sup>fl/fl</sup>xLyz2-cre* BMMs, cells with an additional deletion of *Ripk3* (*Ogt<sup>fl/fl</sup>xLyz2-creRipk3<sup>-/-</sup>*) showed a complete abolishment of the increased cytokine generation (Figures 4B and S6A), as well as of *Nos2* transcript (Figure S6A) and nitric oxide (NO) production (Figure 4C) upon LPS treatment. Furthermore, *Ogt<sup>fl/fl</sup>xLyz2-creRipk3<sup>-/-</sup>* mice, compared with *Ogt<sup>fl/fl</sup>xLyz2-cre* mice, were completely rescued from sepsis-induced lethality (Figure 4D). Consistently, increased production of inflammatory cytokines in septic *Ogt<sup>fl/fl</sup>xLyz2-cre* mice was also abolished in septic *Ogt<sup>fl/fl</sup>xLyz2-creRipk3<sup>-/-</sup>* mice (Figures 4E–4G). In sum, these results suggest that RIPK3 is a key effector that mediates the hyperinflammatory response in *Ogt<sup>fl/fl</sup>xLyz2-cre* cells and mice. We further generated *Ogt<sup>fl/fl</sup>xLyz2-creMkl1<sup>-/-</sup>* mice to examine whether the hyperinflammatory phenotype in *Ogt<sup>fl/fl</sup>xLyz2-cre* macrophages was due to RIPK3-mediated innate immune signaling or secondary to MLKL-mediated necroptosis. *Ogt<sup>fl/fl</sup>xLyz2-creMkl1<sup>-/-</sup>* BMMs produced cytokines (Figures 4H and S6B) and NO (Figure 4I) at the same concentrations as those in *Ogt<sup>fl/fl</sup>xLyz2-cre* macrophages. No improvement in survival rate (Figure 4J) or inflammatory response (Figures 4K and 4L) was observed in *Ogt<sup>fl/fl</sup>xLyz2-creMkl1<sup>-/-</sup>* mice compared with *Ogt<sup>fl/fl</sup>xLyz2-cre* mice during CLP-induced sepsis. In sum, these findings indicate that OGT negatively regulates macrophage cytokine production and septic inflammation by restraining the RIPK3-mediated inflammatory response.

### Increased Necroptosis Response in *Ogt<sup>fl/fl</sup>xLyz2-cre* Macrophages Is Due to RIPK3 Hyperactivation

We next asked whether OGT affects necroptosis signaling through RIPK3. When stimulated with LPS plus the pan-caspase inhibitor zVAD, *Ogt<sup>fl/fl</sup>xLyz2-cre* BMMs exhibited significantly enhanced necroptosis as shown by the increased release of lactate dehydrogenase (LDH) (Figure 5A), high mobility group box 1 (HMGB1), and IL-1 $\alpha$ , as well as augmented phosphorylation

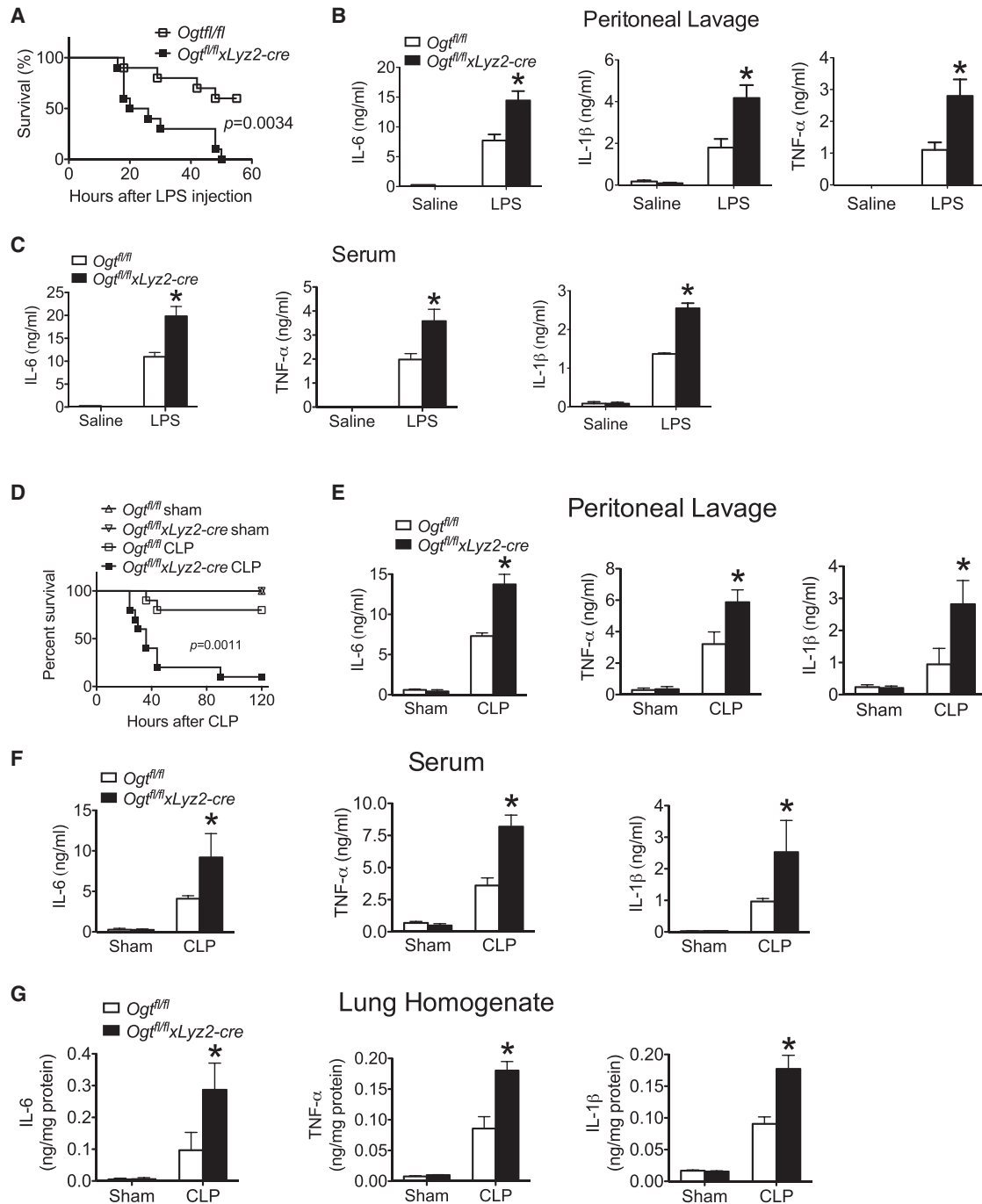


**Figure 3. Myeloid-Derived OGT Protects Mice from Experimental Sepsis**

*Ogt<sup>fl/fl</sup>* and *Ogt<sup>fl/fl</sup>xLyz2-cre* mice were injected intraperitoneally with 15 mg/kg body weight LPS ( $n = 10$  for each group) (A–C) or were subjected to a sham or CLP procedure ( $n = 8$ –10 for each group) (D–G). Survival was recorded (A and D). IL-6, TNF- $\alpha$ , and IL-1 $\beta$  concentrations in peritoneal lavage (B and E), serum (C and F), and lungs homogenates (G) were measured by ELISA 24 h after LPS injection or a CLP procedure. \* $p < 0.05$  versus controls (two-tailed Student's *t* test). Data are from one experiment representative of three experiments (B, C, and E–G; mean  $\pm$  SD) or two experiments (A and F). Please also see Figure S4.

of RIPK3 and MLKL (Figure 5B). RIPK1 phosphorylation was similarly induced between WT and *Ogt<sup>fl/fl</sup>xLyz2-cre* BMMs, indicating that OGT affected activation of RIPK3, but not RIPK1. Compared with WT BMMs, *Ogt<sup>fl/fl</sup>xLyz2-cre* BMMs also showed markedly increased staining of SYTOX Green, a cell-impermeable DNA-

binding fluorescence dye (Orozco et al., 2014), upon treatment with LPS plus zVAD, suggesting increased necroptosis (Figure 5C). We observed a slightly induced LDH release (Figures S6C and S6D) and a low amount of phosphorylated RIPK3 (Figures S6E and S6F) in *Ogt<sup>fl/fl</sup>xLyz2-cre* BMMs upon LPS challenge

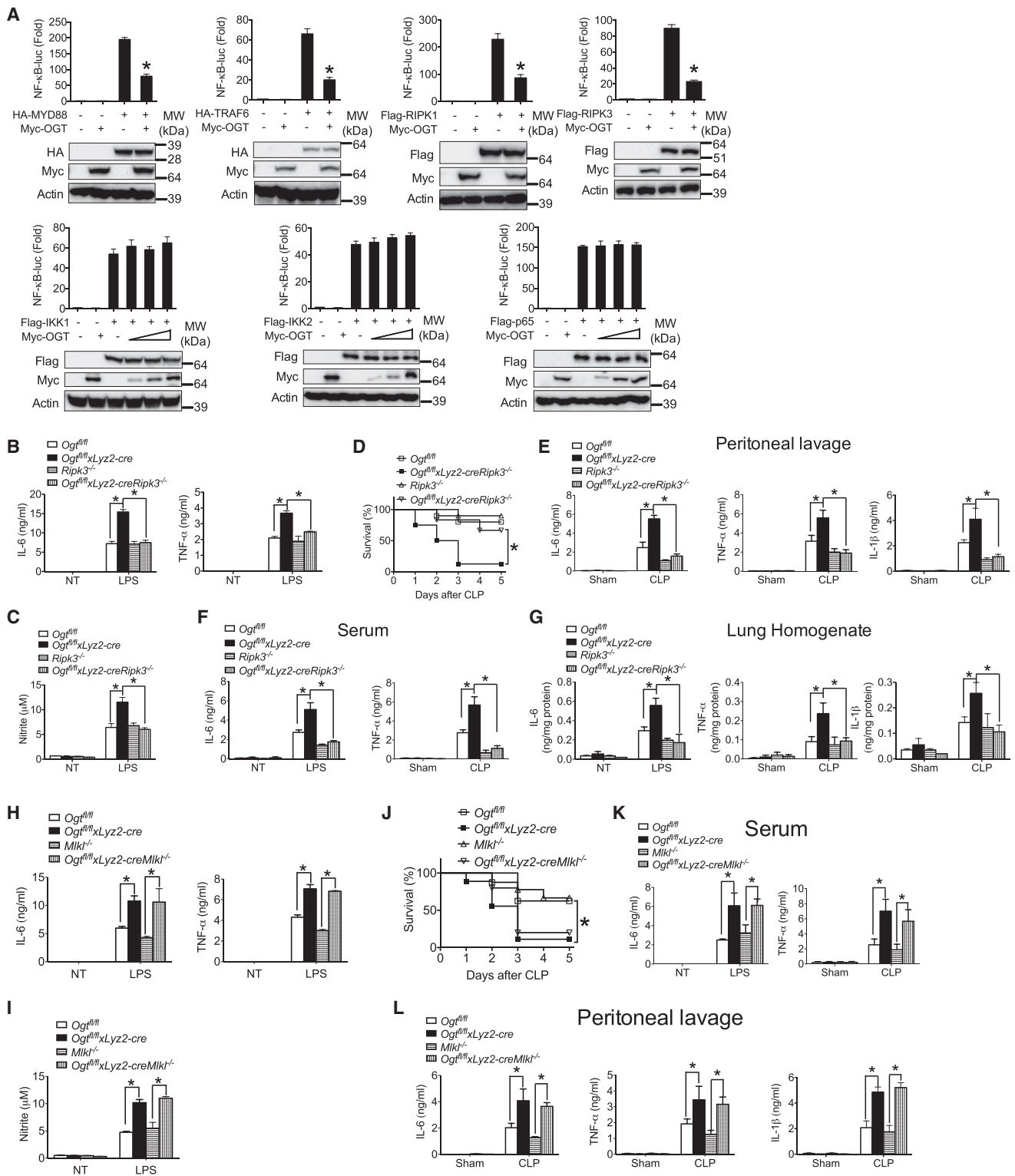


**Figure 4. OGT Inhibits the Innate Immune Responses through RIPK3**

(A) NF- $\kappa$ B-driven luciferase activities by co-expression of MYD88, TRAF6, RIPK1, RIPK3, IKK1, IKK2, or p65 in the presence or absence of the expression plasmid for OGT.

(B and C) IL-6 and TNF- $\alpha$  (B) and nitrite (C) produced by *Ogt<sup>fl/fl</sup>*, *Ogt<sup>fl/fl</sup>xLyz2-cre*, *Ripk3<sup>-/-</sup>*, or *Ogt<sup>fl/fl</sup>xLyz2-creRipk3<sup>-/-</sup>* BMMs stimulated with or without LPS. (D–G) Survival rate (D) and IL-6, TNF- $\alpha$ , and IL-1 $\beta$  in peritoneal lavage (E), serum (F), or lungs (G) in *Ogt<sup>fl/fl</sup>* (n = 14), *Ogt<sup>fl/fl</sup>xLyz2-cre* (n = 10), *Ripk3<sup>-/-</sup>* (n = 12), or *Ogt<sup>fl/fl</sup>xLyz2-creRipk3<sup>-/-</sup>* mice (n = 8) subjected to a CLP procedure.

(legend continued on next page)

alone. Pretreatment with GSK-872, but not Nec-1, completely abolished cell death in both WT and *Ogt<sup>fl/fl</sup>xLyz2-cre* BMMs (Figure 5H). OSML-1 treatment increased necroptosis, which phenocopied *Ogt* genetic deletion (Figure S6G) and required the kinase activity of RIPK3, but not RIPK1 (Figure S6H). Together, these findings suggest that RIPK3 kinase activity is responsible for increased necroptosis in *Ogt<sup>fl/fl</sup>xLyz2-cre* BMMs.

We next used a Transwell co-culture system to examine whether enhanced necroptosis was caused by an altered extracellular cytokine environment for *Ogt<sup>fl/fl</sup>xLyz2-cre* macrophages. Despite the genotypes of cells in the upper chambers, *Ogt<sup>fl/fl</sup>xLyz2-cre* BMMs in the lower chambers showed increased phosphorylation of RIPK3 and MLKL upon stimulation with LPS plus zVAD, supporting a cell-intrinsic mechanism of OGT in affecting the necroptosis (Figure 5D). After the CLP procedure, septic *Ogt<sup>fl/fl</sup>xLyz2-cre* mice contained markedly higher amounts of HMGB1 and IL-1 $\alpha$  in the peritoneal lavage fluids than did septic WT mice (Figure 5E). Upon necroptosis induction, RIPK3 and RIPK1 form an amyloid signaling complex known as the necrosome (Li et al., 2012), which can be biochemically enriched in a NP-40-insoluble cellular fraction (Najjar et al., 2016). We compared necrosome formation between WT and *Ogt<sup>fl/fl</sup>xLyz2-cre* BMMs and found that the appearance of RIPK1, RIPK3, and MLKL in the detergent-insoluble cellular fractions was heavily augmented in *Ogt<sup>fl/fl</sup>xLyz2-cre* BMMs (Figure 5F). Co-immunoprecipitation assays revealed an increased association between endogenous RIPK3 and RIPK1, in either a phosphorylated or total form, in necroptotic *Ogt<sup>fl/fl</sup>xLyz2-cre* BMMs (Figure 5G). These findings support an anti-necroptotic effect of OGT in macrophages.

Compared with *Ogt<sup>fl/fl</sup>xLyz2-cre* BMMs, *Ogt<sup>fl/fl</sup>xLyz2-creRipk3<sup>-/-</sup>* BMMs showed a complete rescue from cell death in response to LPS plus zVAD (Figure 5I) or LPS alone (Figure S6I), as well as the loss of MLKL phosphorylation (Figure 5J). Similarly, *Ogt<sup>fl/fl</sup>xLyz2-creMlkl<sup>-/-</sup>* BMMs were also rescued from cell death (Figures 5K and S5J). Importantly, *Ogt<sup>-/-</sup>* still caused increased RIPK3 phosphorylation in the *Mlkl<sup>-/-</sup>* genetic background (*Ogt<sup>fl/fl</sup>xLyz2-creMlkl<sup>-/-</sup>* versus *Mlkl<sup>-/-</sup>* BMMs) during necroptosis, indicating that OGT affects RIPK3 activity independently of MLKL-mediated cell death (Figure 5L). In sum, these findings suggest that *Ogt<sup>fl/fl</sup>xLyz2-cre* BMMs exhibit an increased necroptotic response, which is dependent on RIPK3. We also tested whether OGT affects apoptosis. Hallmarks of apoptosis, including the drop in intracellular ATP concentration, cleavage of poly (ADP-ribose) polymerase (PARP), and caspase-3, were comparable between WT and *Ogt<sup>fl/fl</sup>xLyz2-cre* BMMs in response to TNF- $\alpha$  plus cycloheximide (Figures S6K and S6L) or staurosporine (Figures S6M and S6N), suggesting no involvement of OGT in either the extrinsic or intrinsic apoptotic pathway. We finally asked whether the inhibitory effect of OGT on RIPK3 phosphorylation and activation occurred in a physiological condition by lowering the glucose concentration in culture medium. Switching the glucose concentration from

25 to 2 mM increased necroptosis in WT BMMs to that observed in *Ogt<sup>fl/fl</sup>xLyz2-cre* BMMs but showed no effect in the cells' lack of RIPK3 or MLKL (Figure 5M). These results indicate that glucose metabolism affects the RIPK3-MLKL necroptosis pathway through OGT.

### O-GlcNAcylation of RIPK3 on T467 Inhibits Inflammation and Necroptosis

We sought to determine whether OGT directly O-GlcNAcylates RIPK3 to affect its function. Immunoprecipitated endogenous RIPK3 exhibited a positive O-GlcNAc signal in WT mouse BMMs, but not *Ogt<sup>fl/fl</sup>xLyz2-cre* BMMs (Figure 6A). Reciprocal precipitation with the use of succinylated wheat germ agglutinin (sWGA) beads, a widely used biochemical strategy for enriching O-GlcNAcylated proteins (Hart et al., 2011), also detected RIPK3 as an O-GlcNAcylated protein (Figure 6B). Both RIPK3 O-GlcNAcylation and the association between RIPK3 and OGT increased upon LPS stimulation (Figure 6C), despite attenuated total protein O-GlcNAcylation (Figure 1I), which suggests that OGT actively and specifically promotes RIPK3 O-GlcNAcylation and prevents its activation. In contrast, necroptosis induction by LPS plus zVAD caused the opposite effects (Figure 6D). As expected, lowering medium glucose concentration from 25 to 2 mM markedly decreased RIPK3 O-GlcNAcylation with or without LPS treatment (Figure 6E). These findings explain the lack of necroptosis in LPS-stimulated WT macrophages and identify diminished RIPK3 O-GlcNAcylation as an important step mediating necroptosis. Indeed, treatment with PUGNAC, a widely used O-GlcNAcylase (OGA) inhibitor that potently enhances protein O-GlcNAcylation (Li et al., 2017), rescued RIPK3 O-GlcNAcylation and attenuated RIPK3 phosphorylation (Figure 6F) and cell necroptosis (Figure 6G).

We next sought to identify the O-GlcNAcylation site(s) on RIPK3. O-GlcNAcylation of exogenously expressed human RIPK3 in 293T cells was sharply enhanced by WT OGT, but not by an enzyme-dead mutant of OGT (K908A) (Lazarus et al., 2011), indicating a requirement of OGT enzymatic activity for RIPK3 O-GlcNAcylation (Figure 6H). O-GlcNAcylation of exogenously expressed mouse *Ripk3* could also be detected in 293T cells (Figure S7A). RIPK3 contains an N-terminal kinase domain and a C-terminal RHIM motif, both of which are necessary for necroptosis signaling. We therefore generated N-terminal (1–310 aa) and C-terminal (311–518 aa) truncated fragments of RIPK3 (Figure 6I) and detected the O-GlcNAcylation on its C-terminal fragment (Figure 6J). Through mass spectrometry (MS) analysis, several potential O-GlcNAcylation sites were detected on both full-length RIPK3 and the C-terminal fragment of RIPK3 (Table S3). A follow-up site-directed mutagenesis strategy allowed us to reveal that a single mutant (T467A) inside the RHIM motif (Figure 6I) lost O-GlcNAc signal without affecting RIPK3 abundance (Figures 6K and 6L). It should be noted that T467 on human RIPK3 is only partially conserved among mammalian species (Figure S7B), suggesting a possibility that

(H and I) IL-6 and TNF- $\alpha$  (H) and nitrite (I) produced by *Ogt<sup>fl/fl</sup>*, *Ogt<sup>fl/fl</sup>xLyz2-cre*, *Mlkl<sup>-/-</sup>* or *Ogt<sup>fl/fl</sup>xLyz2-creMlkl<sup>-/-</sup>* BMMs stimulated with or without LPS. (J–L) Survival rate (J) and IL-6, TNF- $\alpha$ , and IL-1 $\beta$  in serum (K) or peritoneal lavage (L) in *Ogt<sup>fl/fl</sup>* (n = 12), *Ogt<sup>fl/fl</sup>xLyz2-cre* (n = 10), *Mlkl<sup>-/-</sup>* (n = 15), or *Ogt<sup>fl/fl</sup>xLyz2-creMlkl<sup>-/-</sup>* mice (n = 13) mice subjected to a CLP procedure.

\*p < 0.05 versus controls (two-tailed Student's t test in A–C, E–I, K, and L). The results shown are representative of four independent experiments (A–C; mean  $\pm$  SD of four biological replicates) or two experiments (D–L). Please also see Figure S5.

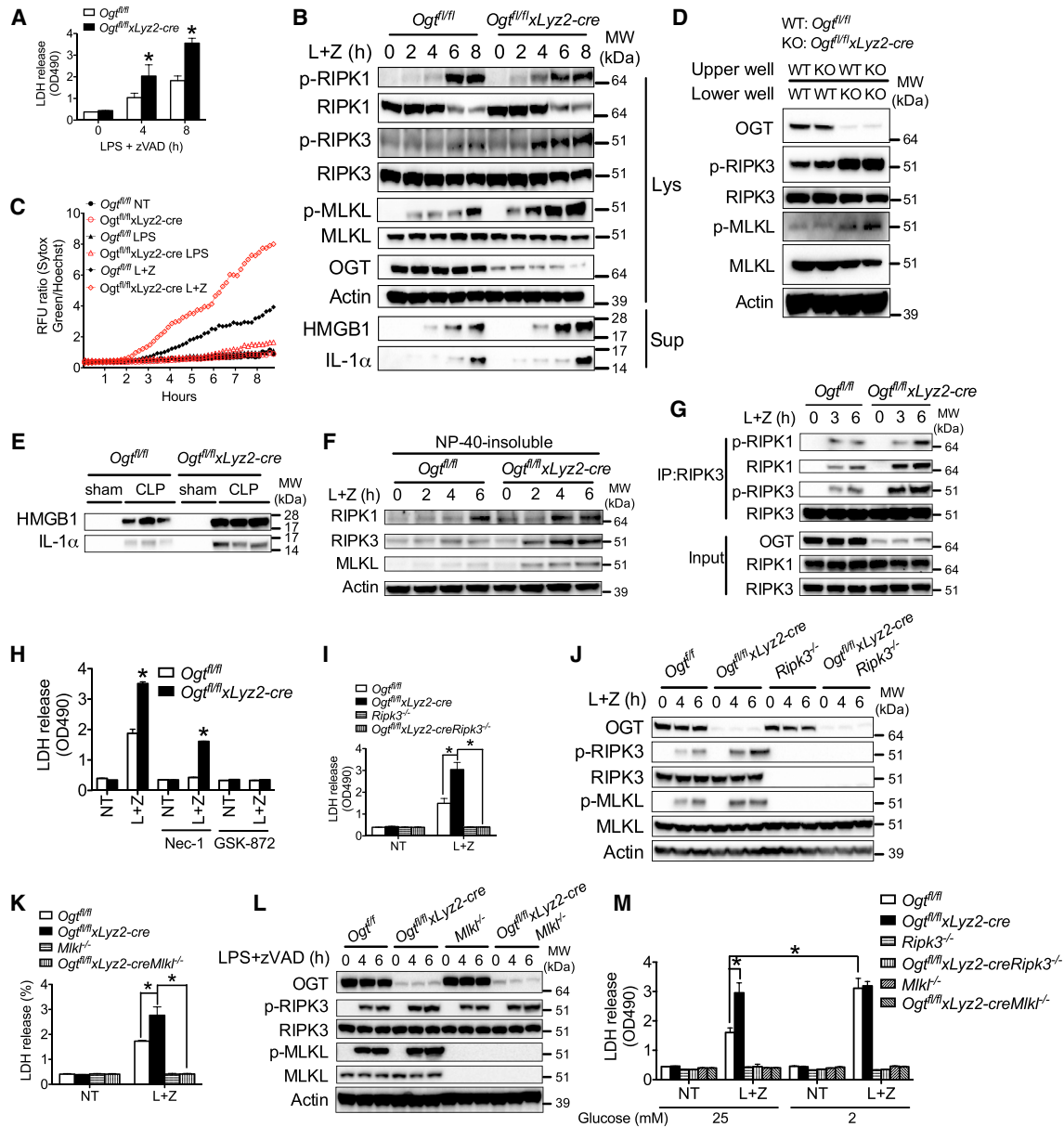


**Figure 5. OGT Inhibits Necroptosis through RIPK3**

(A–C) Cell death assessed by LDH release (A) or Sytox Green staining (C) and phosphorylation of necroptosis signaling molecules (B) in *Ogt<sup>fl/fl</sup>* or *Ogt<sup>fl/fl</sup>xLyz2-cre* BMMs left untreated or stimulated with LPS (200 ng/mL) plus zVAD (10 μM) for the indicated periods.

(D) Immunoblotting of p-RIPK3 and p-MLKL in *Ogt<sup>fl/fl</sup>* or *Ogt<sup>fl/fl</sup>xLyz2-cre* BMMs placed in a Transwell system and stimulated with LPS and zVAD.

(E) Immunoblotting of HMGB1 and IL-1α in the peritoneal lavage fluids of *Ogt<sup>fl/fl</sup>* and *Ogt<sup>fl/fl</sup>xLyz2-cre* mice 24 h after a sham or CLP procedure.

(F–H) Necroptosis signaling molecules in the NP-40-insoluble fractions (F), total or phosphorylated RIPK1 in RIPK3 immunoprecipitates (G), and cell death assessed by LDH release in the absence or presence of RIPK1 inhibitor Nec-1 (20 μM) or RIPK3 inhibitor GSK-872 (10 μM) (H).

(I–M) LDH release (I and K) and phosphorylation of necroptosis signaling molecules (J and L) in *Ogt<sup>fl/fl</sup>*, *Ogt<sup>fl/fl</sup>xLyz2-cre*, *Ripk3<sup>-/-</sup>*, or *Ogt<sup>fl/fl</sup>xLyz2-creRipk3<sup>-/-</sup>* (I and J) and *Mlkl<sup>-/-</sup>* or *Ogt<sup>fl/fl</sup>xLyz2-creMlkl<sup>-/-</sup>* (K and L) BMMs left untreated or stimulated with LPS plus zVAD or placed in culture medium with 2 mM glucose (M).

\**p* < 0.05 versus controls (two-tailed Student's *t* test in A, G, and H). Data represent four independent experiments (A, H, I, K, and M; mean ± SD of four biological replicates) or three experiments (B–G, J, and L). Please also see Figure S6.

additional functional O-GlcNAcylation site(s) could exist in other species.

Given the hyperinflammatory and hyper-necroptotic phenotype of *Ogt<sup>Ameye</sup>* macrophages, we hypothesized that loss of RIPK3 O-GlcNAcylation causes the same effect. Human RIPK3

cannot induce necroptosis in mouse cells because it fails to interact with mouse MLKL (Sun et al., 2012). We therefore used short hairpin RNA (shRNA) to generate *RIPK3*-silenced THP-1 cells and then reconstituted them with either RIPK3 WT or T467A mutant. In response to LPS challenge, *RIPK3*-silenced

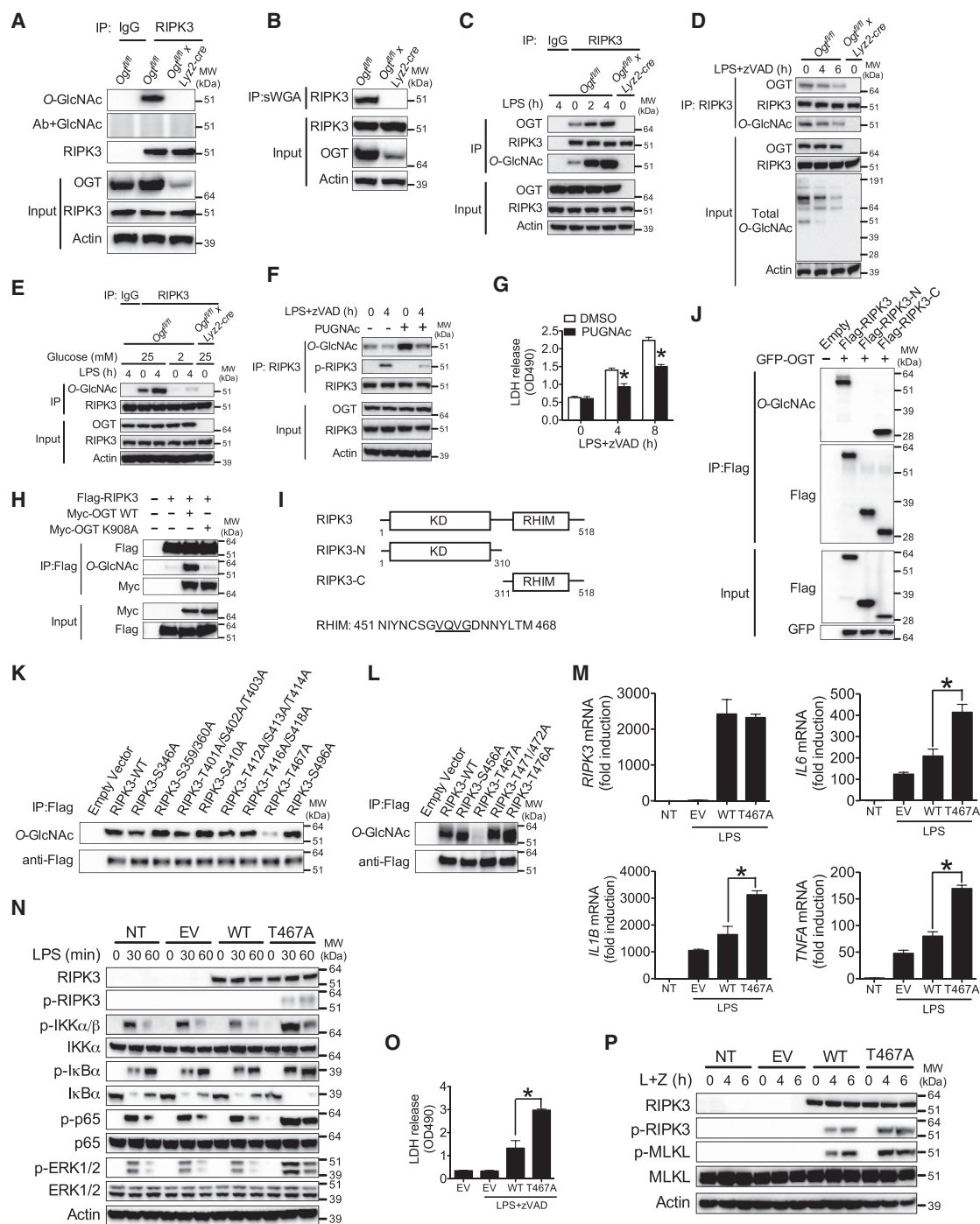


**Figure 6. O-GlcNAcylation of RIPK3 on T467 Suppresses Inflammation and Necroptosis**

(A–G) Total cell lysates of *Ogt<sup>fl/fl</sup>* or *Ogt<sup>fl/fl</sup> × Lyz2-cre* BMDMs left untreated (A and B) or stimulated with LPS alone (C) or LPS plus zVAD (D) with or without PUGNac pretreatment (E). Immunoprecipitation with anti-RIPK3 antibody (A, C–E) or succinylated wheat germ agglutinin (sWGA) beads to pull down O-GlcNAcylated proteins (B).

(H) FLAG-tagged RIPK3 overexpressed in 293T cells together with OGT WT or enzyme-dead K908A mutant was immunoprecipitated with anti-FLAG beads, followed by immunoblotting with anti-O-GlcNAc antibody.

(I) Domain Organization of Human RIPK3 and the RHIM Sequence.

(J) O-GlcNAcylation of the full-length, N-terminal or C-terminal fragments of RIPK3 overexpressed in 293T cells in the presence or absence of WT OGT.

(K and L) O-GlcNAcylation of FLAG-tagged RIPK3 WT or mutants overexpressed in 293T cells together with OGT was analyzed as described in (H).

(legend continued on next page)

cells reconstituted with RIPK3 T467A showed significantly increased cytokine production (Figure 6M), as well as enhanced NF- $\kappa$ B and Erk activation (Figure 6N), in comparison with those reconstituted with WT RIPK3. Because *Ogt<sup>fl/fl</sup> × Lyz2-cre* BMMs failed to show a robust increase in the activation of NF- $\kappa$ B and Erk signaling upon LPS stimulation in comparison with WT BMMs (Figures 2G and 2H), it remains to be determined how RIPK3 activation upon OGT loss triggers increased LPS-induced cytokine responses. Furthermore, compared with WT RIPK3, RIPK3 T467A reconstitution resulted in an augmented necroptosis (Figure 6O) and phosphorylation of RIPK3 and MLKL (Figure 6P). These results demonstrate that RIPK3 O-GlcNAcylation on T467 negatively regulates the innate immune activation and necroptosis response.

### O-GlcNAcylation of RIPK3 on T467 Suppresses Its RHIM Functions

We finally explored the molecular mechanism by which O-GlcNAcylation of RIPK3 antagonizes its functions. The RIPK3 RHIM region has been demonstrated to be essential for both inflammation and the necroptosis pathway (Silke et al., 2015; Wallach et al., 2016), but the kinase activity of RIPK3 is not absolutely required for inflammation (Najjar et al., 2016). We found that overexpressed OGT inhibited RIPK3 phosphorylation in 293T cells (Figure 7A). Given that RIPK3 T467 is localized in the RHIM region, we reasoned that O-GlcNAcylation of RIPK3 on T467 might function by suppressing RHIM-mediated effects, such as RIPK3-RIPK1-hetero- and RIPK3-RIPK3-homo-interaction, as well as RIPK3 kinase activity. Indeed, overexpression of WT OGT, but not OGT-enzyme-dead mutants (K908A and H508A) (Lazarus et al., 2011), efficiently abolished RIPK3-RIPK1-hetero-interaction (Figure 7B), RIPK3-RIPK3-homo-interaction (Figure 7C), and RIPK3 phosphorylation under both conditions. The loss-of-O-GlcNAcylation mutation of RIPK3 (T467A) generated opposite results (Figure 7D). Importantly, the RIPK3 T467A mutant was resistant to OGT-inhibited RIPK3 phosphorylation and RIPK3-RIPK1 interaction. Furthermore, the RIPK3 RHIM mutant (RHIM<sup>mut</sup>) showed defects in both RIPK3-RIPK1 interaction and RIPK3 phosphorylation (Figure 7E), but RIPK3-kinase-dead mutants (D160N and S199A) (McQuade et al., 2013) still interacted with RIPK1 (Figure 7F), supporting the notion that RHIM-mediated RIPK3-RIPK1 interaction is an upstream event leading to RIPK3 phosphorylation. In sum, these findings suggest that OGT-mediated RIPK3 O-GlcNAcylation on T467 suppresses RHIM-mediated RIPK3-RIPK1 interaction and downstream RIPK3 kinase activation.

We next examined whether RIPK3-T467A-induced hyperinflammatory and hyper-necroptotic responses were dependent on the protein's RHIM and/or kinase activity. Both T467A-RHIM<sup>mut</sup> and T467A-S199A double mutants lacked RIPK3 phosphorylation (Figure 7G). Compared with cell reconstitution with RIPK3 T467A, RIPK3-silenced THP-1 cell reconstitution with either RIPK3 T467A-RHIM<sup>mut</sup> or T467A-S199A abolished the

increased cytokine production in response to LPS (Figure 7H) and elevated the necroptotic response (Figure 7I). These findings demonstrate that the loss of O-GlcNAcylation on RIPK3 enhances inflammatory and necroptosis signaling, dependent on RHIM-mediated protein interaction and the resultant kinase activation (Figures S7C–S7F). We further performed structural modeling of RIPK3 by using the I-TASSER program (Yang et al., 2015a) and found that the sidechain of O-GlcNAc at T467 stays in proximity to the RHIM region core amino acids VQVG and most likely perturbs RHIM-mediated protein interaction through steric hinderance (Figure 7J).

## DISCUSSION

Previous studies have provided biochemical evidence to support the notion that O-GlcNAc signaling promotes inflammation. Several key molecules in the TLR-NF- $\kappa$ B signaling pathway have been identified to be O-GlcNAcyated. O-GlcNAcylation of these proteins has been shown to enhance their functional activities and promote the transcription of NF- $\kappa$ B target genes (Ozcan et al., 2010). Our recent study also observed an enhanced inflammatory response and disease severity in chemically induced colitis as a result of attenuated STAT3-IL-10 signaling when OGT expression and enzymatic activity were upregulated in myeloid cells (Li et al., 2017). In this study, we demonstrated an unexpected inhibitory effect of OGT on innate immune activation and necroptosis signaling through RIPK3 O-GlcNAcylation. Therefore, the net effect of OGT-mediated O-GlcNAc signaling in the immune system and inflammation seems to be multifaceted because of the involvement of a variety of target proteins in different immune signaling pathways. Both the increase and decrease in OGT-mediated protein O-GlcNAcylation resulted in a similar hyperinflammatory response through distinct mechanisms. On the one hand, elevated O-GlcNAc signaling promoted activation of the innate immune cells by increasing NF- $\kappa$ B signaling, as well as counteracting the anti-inflammatory STAT3-IL-10 signaling. On the other hand, loss of O-GlcNAc signaling removed an inhibitory mechanism of RIPK3 activation and consequently led to enhanced inflammatory responses and inflammation-associated necroptosis, despite increased IL-10 production. We therefore propose that loss of homeostasis in O-GlcNAc signaling, instead of a simple one-way increase or decrease, is an important metabolic mechanism underlying the pathogenesis of inflammatory diseases.

The aforementioned studies raise an important question on how to regulate OGT-mediated O-GlcNAc signaling under pathophysiological conditions. Previous studies have shed light on two important mechanisms: controlling UDP-GlcNAc availability through regulation of HBP activity and targeting OGT gene transcription and protein degradation. First, the availability of UDP-GlcNAc produced through HBP metabolic processes is an important determinant of OGT enzymatic activity (Hart

(M–P) RIPK3-silenced THP-1 cells were virally transfected with RIPK3 WT or T467A mutant, followed by LPS (M and N) or LPS plus zVAD (O and P) stimulation. Transcripts of *RIPK3*, *IL6*, *TNFA*, and *IL1B* (M), total and phosphorylated RIPK3, Erk, IKK $\alpha/\beta$ , I $\kappa$ B $\alpha$  and p65 (N) or necroptosis signaling molecules (P), and LDH release (O) was assayed. \* $p < 0.05$ , versus controls (two-tailed Student's t test (L and N)). Data are from one experiment representative of three independent experiments (A–G, I, J, K, M and O) or four experiments (L and N; mean  $\pm$  SD of three biological replicates). Please also see Figure S7.

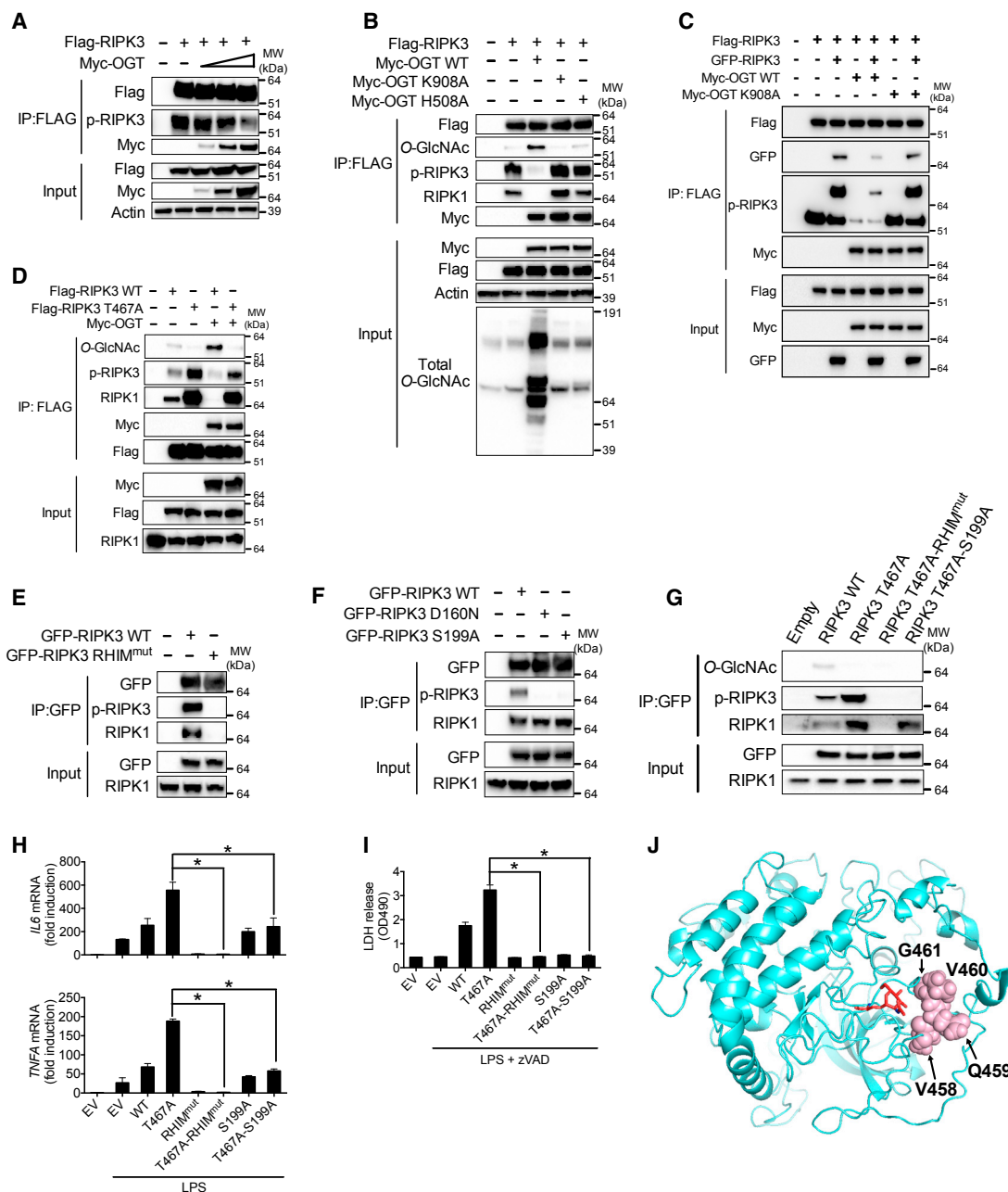


**Figure 7. O-GlcNAcylation of RIPK3 Inhibits RHIM-Mediated RIPK3-RIPK1 Interaction**

(A–D) FLAG-tagged RIPK3 was overexpressed in 293T cells together with the indicated expression plasmids. Immunoprecipitation with anti-FLAG beads, followed by immunoblotting with specific antibodies against O-GlcNAc, p-RIPK3, RIPK1, and GFP, was performed.

(E–G) GFP-tagged RIPK3 WT or mutants were overexpressed in 293T cells. Immunoprecipitation with anti-GFP beads, followed by immunoblotting with specific antibodies against O-GlcNAc, p-RIPK3, or RIPK1, was performed.

(H and I) Transcripts of *IL6* and *TNFA* (H) and LDH release (I) from *RIPK3*-silenced THP-1 cells virally transfected with RIPK3 WT or various mutants and then stimulated with LPS (H) or LPS plus zVAD (I).

(J) Structural modeling of RIPK3 by the I-TASSER program. O-GlcNAcylated T467 is red, and the amino acids VQVG of the RHIM motif are highlighted as pink spheres.

\* $p < 0.05$  versus controls (two-tailed Student's *t* test in G and H). Data are from one experiment representative of three experiments (A–F) or four experiments (H and I; mean  $\pm$  SD of four biological replicates).

et al., 2011). The first and rate-limiting enzyme in HBP, glutamine fructose-6-phosphate transaminase (GFPT), represents a key mediator in affecting downstream OGT signaling by determining UDP-GlcNAc concentration. A recent study reported that GFPT is transcriptionally upregulated under endoplasmic reticulum (ER) stress, and this upregulation leads to increased protein O-GlcNAcylation and provides a protective effect against ischemia-reperfusion injury in the heart (Wang et al., 2014). Our study observed decreased HBP activity and protein O-GlcNAcylation by TLR4 activation, despite increased glycolysis and PPP metabolic activities. In contrast, in a parallel study, we observed increased HBP flux activity and protein O-GlcNAcylation when retinoic-acid-inducible gene I (RIG-I) was activated by intracellular RNA ligands (Li et al., 2018). The opposite O-GlcNAc signaling changes due to activation of distinct innate immune sensors highlight that GFPT-mediated HBP activity is an important mechanism regulating OGT function. How GFPT-controlled HBP activity is differentially regulated during activation of distinct pathogen-recognition-receptor signaling requires further investigation. Second, the abundance of OGT protein is negatively regulated by a ubiquitination-mediated protein-degradation process (Yang et al., 2015b), whereas OGT gene expression is promoted by the transcriptional activity of Nrf2 (Li et al., 2017). Whether OGT function is affected by K63-linked protein ubiquitination, a well-established protein modification for signal transduction, has not been determined yet. In sum, similar to diverse functions of OGT through the targeting of multiple downstream targets, upstream mechanisms that modulate OGT function are also diversified.

Recent studies have identified several intracellular amyloid signaling complexes, including the necrosome (Li et al., 2012), ASC inflammasome (Lu et al., 2014), and MAVS signalosome (Cai et al., 2014), which initiate distinct important innate immune signaling. One common feature of these high-molecular-weight complexes is well-characterized protein-protein binding patterns depending on unique domains on each protein component. The RHIM region of RIPK3, one of the best-studied protein-binding motifs, has been shown to be required for the formation of the necrosome and execution of necroptosis. Depending on which initial sensors receive extracellular or intracellular signals, RIPK3 can directly bind to TRIF (Kaiser et al., 2013), RIPK1 (Li et al., 2012; Mompeán et al., 2018), or ZBP1 (Z-DNA binding protein 1, also known as DAI) (Lin et al., 2016; Newton et al., 2016) through the RHIM motif to activate necroptosis. Recent studies suggest that, in addition to playing a central role in necroptosis, RIPK3 also contributes to activation of the immune response in cell-death-dependent and -independent manners (Alvarez-Diaz et al., 2016; Moriwaki et al., 2017; Najjar et al., 2016). The RIPK3 RHIM motif is critical for both necroptosis and the inflammatory response both *in vitro* and *in vivo*. Our study identified RIPK3 T467, which is located in proximity to the RHIM region core amino acids VQVG, as an O-GlcNAcylation site. Loss of this O-GlcNAcylation promoted RHIM-mediated RIPK3-RIPK1-hetero- and RIPK3-RIPK3-homo-interaction, RIPK3 activation, downstream inflammatory and necroptosis signaling, and cytokine storm in experimental sepsis. These findings support an essential role of RHIM-mediated assembly of the necrosome signaling complex in promoting immune activation and tissue damage in inflammatory diseases such as sepsis.

Previous studies have reported that activated RIPK3 in macrophages deficient in apoptosis-associated molecules (caspase-8 or inhibitors of apoptosis) could activate inflammasomes in response to LPS alone (Galluzzi et al., 2017; Weinlich et al., 2017). Inflammasome activation leads to caspase-1 activation and release of proinflammatory cytokines IL-1 $\beta$  and IL-18, among other substrates (Davis et al., 2011). Both canonical and noncanonical inflammasomes have been indicated to play important roles promoting septic inflammation. We observed that upon LPS stimulation, loss of OGT-mediated O-GlcNAcylation caused RIPK3 phosphorylation and activation, indicating that OGT deficiency might increase RIPK3-dependent IL-1 $\beta$  production. Indeed, we observed increased IL-1 $\beta$  concentration in septic *Ogt<sup>fl/fl</sup>xLyz2-cre* mice, which could be reversed by *Ripk3* deletion. Because IL-1 $\beta$  is a prototypical pyrogen to drive cytokine storm and tissue damage in sepsis, excessive IL-1 $\beta$  could contribute to elevated mortality in septic *Ogt<sup>Δmye</sup>* mice. In sum, our results provide a mechanistical link between OGT-mediated glucose metabolism and key immune signaling in the innate immune system and expand our current understanding of metabolic regulation of the immune function and inflammation-associated diseases. Targeting RIPK3 O-GlcNAcylation presents a potential therapeutic strategy for combating multiple inflammatory diseases.

## STAR★METHODS

Detailed methods are provided in the online version of this paper and include the following:

- KEY RESOURCES TABLE
- CONTACT FOR REAGENT AND RESOURCE SHARING
- EXPERIMENTAL MODEL AND SUBJECT DETAILS
  - Mice
- METHOD DETAILS
  - Reagents and antibodies
  - Cell culture and stimulation
  - RT-PCR
  - Immunoblotting
  - ELISA
  - Nitrite quantitation
  - Experimental sepsis animal models
  - Plasmids and molecular cloning
  - Cell transfection
  - Luciferase assay
  - Metabolomics
  - Nuclear Magnetic Resonance (NMR) Spectroscopy analysis of <sup>13</sup>C-glucose metabolism
  - RIPK3 O-GlcNAcylation site mapping
  - RIPK3 structure prediction
  - Statistics

## SUPPLEMENTAL INFORMATION

Supplemental Information includes seven figures and six tables and can be found with the article online at <https://doi.org/10.1016/j.immuni.2019.01.007>.

## ACKNOWLEDGMENTS

We thank A.S. Baldwin for the NF- $\kappa$ B-driven luciferase reporter construct and the expression plasmids for IKK1, IKK2, and RELA; F.K. Chan for the RIPK3

WT and mutant expression plasmids; H.K. Lin for the TRAF6 expression plasmid; X. Yu for the OGT expression plasmid; E.S. Mocarski for *Ripk3*<sup>K51A</sup> bone marrow cells; V.M. Dixit for *Ripk3*<sup>-/-</sup> mice; J.M. Murphy for *Mlkl*<sup>-/-</sup> mice; and M. Yuan for the metabolomics assay. This work was supported by National Institutes of Health (NIH) grants R01GM120496 to H.W.; 5P01CA120964 and 5P30CA006516 to J.M.A.; P30CA016086 to the UNC Lineberger Comprehensive Cancer Center; R01CA163649, R01CA210439, and R01CA216853 to P.K.S.; P30GM103335 and P20GM113126 to R.P.; R00DE024173 and R01DE026728 to Y.L.L.; R01DK102648 to X.Y.; and R37AI044828 and R35CA231620 to D.R.G. Metabolic tracer experiments were performed in facilities renovated under NIH grant RR015468-01.

## AUTHOR CONTRIBUTIONS

X.L., W.G., and H.W. designed the experiments; X.L., W.G., H.W., T.L., R.E.L., and A.C.K. performed experiments and provided intellectual input; L.E.H. performed key mass spectrometry experiments; J.M.A., K.S.A., and P.K.S. performed key metabolomics experiments and provided intellectual input; F.B. and R.P. performed key metabolic tracer experiments; G.Y. performed structural modeling of human RIPK3; Y.L.L. and X.Y. contributed intellectual input and generated critical reagents; D.A.R., M.Y., and D.R.G. generated critical reagents and provided intellectual input; and H.W. supervised the study, interpreted the data, and wrote the manuscript.

## DECLARATION OF INTERESTS

The authors declare no competing financial interests.

Received: July 3, 2018

Revised: November 21, 2018

Accepted: January 15, 2019

Published: February 12, 2019

## REFERENCES

- Alvarez-Diaz, S., Dillon, C.P., Lalaoui, N., Tanzer, M.C., Rodriguez, D.A., Lin, A., Lebois, M., Hakem, R., Josefsson, E.C., O'Reilly, L.A., et al. (2016). The pseudokinase MLKL and the kinase RIPK3 have distinct roles in autoimmune disease caused by loss of death-receptor-induced apoptosis. *Immunity* **45**, 513–526.
- Arts, R.J., Novakovic, B., Ter Horst, R., Carvalho, A., Bekkering, S., Lachmandas, E., Rodrigues, F., Silvestre, R., Cheng, S.C., Wang, S.Y., et al. (2016). Glutaminolysis and fumarate accumulation integrate immunometabolic and epigenetic programs in trained immunity. *Cell Metab.* **24**, 807–819.
- Ashburner, B.P., Westerheide, S.D., and Baldwin, A.S., Jr. (2001). The p65 (RelA) subunit of NF- $\kappa$ B interacts with the histone deacetylase (HDAC) corepressors HDAC1 and HDAC2 to negatively regulate gene expression. *Mol. Cell Biol.* **21**, 7065–7077.
- Bambouskova, M., Gorvel, L., Lampropoulou, V., Sergushichev, A., Loginicheva, E., Johnson, K., Korenfeld, D., Mathyer, M.E., Kim, H., Huang, L.H., et al. (2018). Electrophilic properties of itaconate and derivatives regulate the I $\kappa$ B $\zeta$ -ATF3 inflammatory axis. *Nature* **556**, 501–504.
- Berger, S.B., Kasparcova, V., Hoffman, S., Swift, B., Dare, L., Schaeffer, M., Capriotti, C., Cook, M., Finger, J., Hughes-Earle, A., et al. (2014). Cutting Edge: RIP1 kinase activity is dispensable for normal development but is a key regulator of inflammation in SHARPIN-deficient mice. *J. Immunol.* **192**, 5476–5480.
- Buck, M.D., Sowell, R.T., Kaech, S.M., and Pearce, E.L. (2017). Metabolic instruction of immunity. *Cell* **169**, 570–586.
- Cai, X., Chen, J., Xu, H., Liu, S., Jiang, Q.X., Halfmann, R., and Chen, Z.J. (2014). Prion-like polymerization underlies signal transduction in antiviral immune defense and inflammasome activation. *Cell* **156**, 1207–1222.
- Chen, Q., Chen, Y., Bian, C., Fujiki, R., and Yu, X. (2013). TET2 promotes histone O-GlcNAcylation during gene transcription. *Nature* **493**, 561–564.
- Davis, B.K., Wen, H., and Ting, J.P. (2011). The inflammasome NLRs in immunity, inflammation, and associated diseases. *Annu. Rev. Immunol.* **29**, 707–735.
- Degterev, A., Hitomi, J., Grzescheid, M., Ch'en, I.L., Korkina, O., Teng, X., Abbott, D., Cuny, G.D., Yuan, C., Wagner, G., et al. (2008). Identification of RIP1 kinase as a specific cellular target of necrostatins. *Nat. Chem. Biol.* **4**, 313–321.
- Delaglio, F., Grzesiek, S., Vuister, G.W., Zhu, G., Pfeifer, J., and Bax, A. (1995). NMRPipe: a multidimensional spectral processing system based on UNIX pipes. *J. Biomol. NMR* **6**, 277–293.
- Everts, B., Amiel, E., Huang, S.C., Smith, A.M., Chang, C.H., Lam, W.Y., Redmann, V., Freitas, T.C., Blagih, J., van der Windt, G.J., et al. (2014). TLR-driven early glycolytic reprogramming via the kinases TBK1-IKK $\epsilon$  supports the anabolic demands of dendritic cell activation. *Nat. Immunol.* **15**, 323–332.
- Galluzzi, L., Kepp, O., Chan, F.K., and Kroemer, G. (2017). Necroptosis: mechanisms and relevance to disease. *Annu. Rev. Pathol.* **12**, 103–130.
- Gunda, V., Yu, F., and Singh, P.K. (2016). Validation of metabolic alterations in microscale cell culture lysates using hydrophilic interaction liquid chromatography (HILIC)-tandem mass spectrometry-based metabolomics. *PLoS ONE* **11**, e0154416.
- Hart, G.W., Slawson, C., Ramirez-Correa, G., and Lagerlof, O. (2011). Cross talk between O-GlcNAcylation and phosphorylation: roles in signaling, transcription, and chronic disease. *Annu. Rev. Biochem.* **80**, 825–858.
- Hotchkiss, R.S., Monneret, G., and Payen, D. (2013). Sepsis-induced immunosuppression: from cellular dysfunctions to immunotherapy. *Nat. Rev. Immunol.* **13**, 862–874.
- Johnson, B.A. (2018). From raw data to protein backbone chemical shifts using NMRFX processing and NMRViewJ analysis. *Methods Mol. Biol.* **1688**, 257–310.
- Kaiser, W.J., Sridharan, H., Huang, C., Mandal, P., Upton, J.W., Gough, P.J., Sehon, C.A., Marquis, R.W., Bertin, J., and Mocarski, E.S. (2013). Toll-like receptor 3-mediated necrosis via TRIF, RIP3, and MLKL. *J. Biol. Chem.* **288**, 31268–31279.
- Lazarus, M.B., Nam, Y., Jiang, J., Sliz, P., and Walker, S. (2011). Structure of human O-GlcNAc transferase and its complex with a peptide substrate. *Nature* **469**, 564–567.
- Lei, Y., Wen, H., Yu, Y., Taxman, D.J., Zhang, L., Widman, D.G., Swanson, K.V., Wen, K.W., Damania, B., Moore, C.B., et al. (2012). The mitochondrial proteins NLRX1 and TUFM form a complex that regulates type I interferon and autophagy. *Immunity* **36**, 933–946.
- Levine, Z.G., and Walker, S. (2016). The biochemistry of O-GlcNAc transferase: which functions make it essential in mammalian cells? *Annu. Rev. Biochem.* **85**, 631–657.
- Li, J., McQuade, T., Siemer, A.B., Napetschnig, J., Moriwaki, K., Hsiao, Y.S., Damko, E., Moquin, D., Walz, T., McDermott, A., et al. (2012). The RIP1/RIP3 necrosome forms a functional amyloid signaling complex required for programmed necrosis. *Cell* **150**, 339–350.
- Li, X., Zhang, Z., Li, L., Gong, W., Lazenby, A.J., Swanson, B.J., Herring, L.E., Asara, J.M., Singer, J.D., and Wen, H. (2017). Myeloid-derived cullin 3 promotes STAT3 phosphorylation by inhibiting OGT expression and protects against intestinal inflammation. *J. Exp. Med.* **214**, 1093–1109.
- Li, T., Li, X., Attri, K.S., Liu, C., Li, L., Herring, L.E., Asara, J.M., Lei, Y.L., Singh, P.K., Gao, C., and Wen, H. (2018). O-GlcNAc transferase links glucose metabolism to MAVS-mediated antiviral innate immunity. *Cell Host Microbe* **24**, 791–803.e6.
- Lin, J., Kumari, S., Kim, C., Van, T.M., Wachsmuth, L., Polykratis, A., and Pasparakis, M. (2016). RIPK1 counteracts ZBP1-mediated necroptosis to inhibit inflammation. *Nature* **540**, 124–128.
- Liu, P.S., Wang, H., Li, X., Chao, T., Teav, T., Christen, S., Di Conza, G., Cheng, W.C., Chou, C.H., Vavakova, M., et al. (2017).  $\alpha$ -ketoglutarate orchestrates macrophage activation through metabolic and epigenetic reprogramming. *Nat. Immunol.* **18**, 985–994.
- Lu, A., Magupalli, V.G., Ruan, J., Yin, Q., Atianand, M.K., Vos, M.R., Schröder, G.F., Fitzgerald, K.A., Wu, H., and Egelman, E.H. (2014). Unified polymerization mechanism for the assembly of ASC-dependent inflammasomes. *Cell* **156**, 1193–1206.

- Mandal, P., Berger, S.B., Pillay, S., Moriwaki, K., Huang, C., Guo, H., Lich, J.D., Finger, J., Kasparcova, V., Votta, B., et al. (2014). RIP3 induces apoptosis independent of pro-necrotic kinase activity. *Mol. Cell* **56**, 481–495.
- McQuade, T., Cho, Y., and Chan, F.K. (2013). Positive and negative phosphorylation regulates RIP1- and RIP3-induced programmed necrosis. *Biochem. J.* **456**, 409–415.
- Mills, E.L., Ryan, D.G., Prag, H.A., Dikovskaya, D., Menon, D., Zaslona, Z., Jedrychowski, M.P., Costa, A.S.H., Higgins, M., Hams, E., et al. (2018). Itaconate is an anti-inflammatory metabolite that activates Nrf2 via alkylation of KEAP1. *Nature* **556**, 113–117.
- Mompeán, M., Li, W., Li, J., Laage, S., Siemer, A.B., Bozkurt, G., Wu, H., and McDermott, A.E. (2018). The structure of the necrosome RIPK1-RIPK3 core, a human hetero-amyloid signaling complex. *Cell* **173**, 1244–1253.e10.
- Moriwaki, K., Balaji, S., Bertin, J., Gough, P.J., and Chan, F.K. (2017). Distinct kinase-independent role of RIPK3 in CD11c<sup>+</sup> mononuclear phagocytes in cytokine-induced tissue repair. *Cell Rep.* **18**, 2441–2451.
- Murphy, J.M., Czabotar, P.E., Hildebrand, J.M., Lucet, I.S., Zhang, J.G., Alvarez-Diaz, S., Lewis, R., Lalaoui, N., Metcalf, D., Webb, A.L., et al. (2013). The pseudokinase MLKL mediates necroptosis via a molecular switch mechanism. *Immunity* **39**, 443–453.
- Najjar, M., Saleh, D., Zelic, M., Nogusa, S., Shah, S., Tai, A., Finger, J.N., Polykratis, A., Gough, P.J., Bertin, J., et al. (2016). RIPK1 and RIPK3 kinases promote cell-death-independent inflammation by Toll-like receptor 4. *Immunity* **45**, 46–59.
- Newton, K., Sun, X., and Dixit, V.M. (2004). Kinase RIP3 is dispensable for normal NF- $\kappa$ B signaling by the B-cell and T-cell receptors, tumor necrosis factor receptor 1, and Toll-like receptors 2 and 4. *Mol. Cell Biol.* **24**, 1464–1469.
- Newton, K., Wickliffe, K.E., Maltzman, A., Dugger, D.L., Strasser, A., Pham, V.C., Lill, J.R., Roose-Girma, M., Warming, S., Solon, M., et al. (2016). RIPK1 inhibits ZBP1-driven necroptosis during development. *Nature* **540**, 129–133.
- O'Neill, L.A., Kishton, R.J., and Rathmell, J. (2016). A guide to immunometabolism for immunologists. *Nat. Rev. Immunol.* **16**, 553–565.
- Orozco, S., Yatim, N., Werner, M.R., Tran, H., Gunja, S.Y., Tait, S.W., Albert, M.L., Green, D.R., and Oberst, A. (2014). RIPK1 both positively and negatively regulates RIPK3 oligomerization and necroptosis. *Cell Death Differ.* **21**, 1511–1521.
- Ozcan, S., Andrali, S.S., and Cantrell, J.E. (2010). Modulation of transcription factor function by O-GlcNAc modification. *Biochim. Biophys. Acta* **1799**, 353–364.
- Pathak, S., Borodkin, V.S., Albarbarawi, O., Campbell, D.G., Ibrahim, A., and van Aalten, D.M. (2012). O-GlcNAcylation of TAB1 modulates TAK1-mediated cytokine release. *EMBO J.* **31**, 1394–1404.
- Shafi, R., Iyer, S.P., Ellies, L.G., O'Donnell, N., Marek, K.W., Chui, D., Hart, G.W., and Marth, J.D. (2000). The O-GlcNAc transferase gene resides on the X chromosome and is essential for embryonic stem cell viability and mouse ontogeny. *Proc. Natl. Acad. Sci. USA* **97**, 5735–5739.
- Siddiquee, K., Zhang, S., Guida, W.C., Blaskovich, M.A., Greedy, B., Lawrence, H.R., Yip, M.L., Jove, R., McLaughlin, M.M., Lawrence, N.J., et al. (2007). Selective chemical probe inhibitor of Stat3, identified through structure-based virtual screening, induces antitumor activity. *Proc. Natl. Acad. Sci. USA* **104**, 7391–7396.
- Silke, J., Rickard, J.A., and Gerlic, M. (2015). The diverse role of RIP kinases in necroptosis and inflammation. *Nat. Immunol.* **16**, 689–697.
- Su, H., Bidère, N., Zheng, L., Cubre, A., Sakai, K., Dale, J., Salmena, L., Hakem, R., Straus, S., and Lenardo, M. (2005). Requirement for caspase-8 in NF- $\kappa$ B activation by antigen receptor. *Science* **307**, 1465–1468.
- Sun, L., Wang, H., Wang, Z., He, S., Chen, S., Liao, D., Wang, L., Yan, J., Liu, W., Lei, X., and Wang, X. (2012). Mixed lineage kinase domain-like protein mediates necrosis signaling downstream of RIP3 kinase. *Cell* **148**, 213–227.
- Tannahill, G.M., Curtis, A.M., Adamik, J., Palsson-McDermott, E.M., McGettrick, A.F., Goel, G., Frezza, C., Bernard, N.J., Kelly, B., Foley, N.H., et al. (2013). Succinate is an inflammatory signal that induces IL-1 $\beta$  through HIF-1 $\alpha$ . *Nature* **496**, 238–242.
- Wallach, D., Kang, T.B., Dillon, C.P., and Green, D.R. (2016). Programmed necrosis in inflammation: Toward identification of the effector molecules. *Science* **352**, aaf2154.
- Wang, Z.V., Deng, Y., Gao, N., Pedrozo, Z., Li, D.L., Morales, C.R., Criollo, A., Luo, X., Tan, W., Jiang, N., et al. (2014). Spliced X-box binding protein 1 couples the unfolded protein response to hexosamine biosynthetic pathway. *Cell* **156**, 1179–1192.
- Weinlich, R., Oberst, A., Beere, H.M., and Green, D.R. (2017). Necroptosis in development, inflammation and disease. *Nat. Rev. Mol. Cell Biol.* **18**, 127–136.
- Wen, H., Lei, Y., Eun, S.Y., and Ting, J.P. (2010). Plexin-A4-semaphorin 3A signaling is required for Toll-like receptor- and sepsis-induced cytokine storm. *J. Exp. Med.* **207**, 2943–2957.
- Yang, W.-L., Wang, J., Chan, C.-H., Lee, S.-W., Campos, A.D., Lamothe, B., Hur, L., Grabiner, B.C., Lin, X., Darnay, B.G., and Lin, H.-K. (2009). The E3 ligase TRAF6 regulates Akt ubiquitination and activation. *Science* **325**, 1134–1138.
- Yang, X., and Qian, K. (2017). Protein O-GlcNAcylation: emerging mechanisms and functions. *Nat. Rev. Mol. Cell Biol.* **18**, 452–465.
- Yang, J., Yan, R., Roy, A., Xu, D., Poisson, J., and Zhang, Y. (2015a). The I-TASSER Suite: protein structure and function prediction. *Nat. Methods* **12**, 7–8.
- Yang, Y., Yin, X., Yang, H., and Xu, Y. (2015b). Histone demethylase LSD2 acts as an E3 ubiquitin ligase and inhibits cancer cell growth through promoting proteasomal degradation of OGT. *Mol. Cell* **58**, 47–59.
- Yang, Y.R., Kim, D.H., Seo, Y.K., Park, D., Jang, H.J., Choi, S.Y., Lee, Y.H., Lee, G.H., Nakajima, K., Taniguchi, N., et al. (2015c). Elevated O-GlcNAcylation promotes colonic inflammation and tumorigenesis by modulating NF- $\kappa$ B signaling. *Oncotarget* **6**, 12529–12542.

## STAR★METHODS

## KEY RESOURCES TABLE

REAGENT or RESOURCE	SOURCE	IDENTIFIER
Antibodies		
Rabbit polyclonal anti-OGT	Cell Signaling Technology	Cat#5368; RRID: AB_11217621
Mouse monoclonal anti-O-GlcNAc	Cell Signaling Technology	Cat#9875; RRID: AB_10950973
Rabbit polyclonal anti-NOS2	EMD Millipore	Cat#ABN26; RRID: AB_10805939
Rabbit polyclonal anti-mouse-phospho-RIPK1 (Ser166)	Cell Signaling Technology	Cat#31122
Rabbit monoclonal anti-RIPK1	Cell Signaling Technology	Cat#3493; RRID: AB_2305314
Rabbit anti-mouse-phospho-RIPK3 (Thr231, Ser232)	Genentech	GEN135-35-9
Rabbit anti-human-phospho-RIPK3 (Ser227)	Abcam	Cat#ab209384; RRID: AB_2714035
Rabbit anti-RIPK3	Novus	Cat#NBP1-77299; RRID: AB_11040928
Rabbit monoclonal anti-mouse-phospho-MLKL (Ser345)	Abcam	Cat#ab196436; RRID: AB_2687465
Rabbit polyclonal anti-mouse MLKL	Abgent	Cat#AP14272b; RRID: AB_11134649
Rabbit monoclonal anti-Human-phospho-MLKL (Ser358)	Abcam	Cat#ab187091; RRID: AB_2619685
Rabbit polyclonal anti-Human MLKL	Cell Signaling Technology	Cat#14993; RRID: AB_2721822
Rabbit polyclonal anti-HMGB1	Abcam	Cat#ab18256; RRID: AB_444360
Goat polyclonal anti-mouse-IL-1 $\alpha$	R and D Systems	Cat#AF-400-NA; RRID: AB_354473
Rabbit monoclonal anti-phospho-p44/42 MAPK (Erk1/2) (Thr202/Tyr204)	Cell Signaling Technology	Cat#4370; RRID: AB_2315112
Rabbit monoclonal anti-p44/42 MAPK (Erk1/2)	Cell Signaling Technology	Cat#4695; RRID: AB_390779
Rabbit monoclonal anti-phospho-SAPK/JNK (Thr183/Tyr185)	Cell Signaling Technology	Cat#4668; RRID: AB_823588
Goat polyclonal anti-JNK1	Santa Cruz Biotechnology	Cat#sc-474-G; RRID: AB_632384
Rabbit polyclonal anti-phospho-p38 MAPK (Thr180/Tyr182)	Cell Signaling Technology	Cat#9211
Rabbit polyclonal anti-p38 MAPK	Cell Signaling Technology	Cat#8690; RRID: AB_10999090
Rabbit monoclonal anti-phospho-IKK $\alpha$ / $\beta$ (Ser176/180)	Cell Signaling Technology	Cat#2697; RRID: AB_2079382
Rabbit polyclonal anti-IKK $\alpha$	EMD Millipore	Cat#07-1107
Rabbit monoclonal anti-phospho-NF- $\kappa$ B p65 (Ser536)	Cell Signaling Technology	Cat#3033; RRID: AB_331284
Rabbit monoclonal anti-NF- $\kappa$ B p65	Cell Signaling Technology	Cat#8242; RRID: AB_10859369
Rabbit monoclonal anti-phospho-I $\kappa$ B $\alpha$ (Ser32)	Cell Signaling Technology	Cat#2859; RRID: AB_561111
RelB	Santa Cruz Biotechnology	Cat#sc-226; RRID: AB_632341
NF- $\kappa$ B1 p105/p50	Cell Signaling Technology	Cat#13586; RRID: AB_2665516
Rabbit polyclonal anti-I $\kappa$ B $\alpha$	Cell Signaling Technology	Cat#9242S; RRID: AB_10694550
Arginase I	BD Biosciences	Cat#610708; RRID: AB_398031
Caspase 8	Cell Signaling Technology	Cat#4927; RRID: AB_2068301
FITC conjugated anti-mouse CD3e	eBioscience	Cat#11-0031-63; RRID: AB_464880
PE-Cy7 conjugated anti-mouse CD4	eBioscience	Cat#25-0041-82; RRID: AB_469576
APC conjugated anti-mouse CD8	BioLegend	Cat#100712; RRID: AB_312751
Mouse monoclonal anti-GFP	Santa Cruz Biotechnology	Cat#sc-9996; RRID: AB_627695
Mouse monoclonal anti-Actin	Santa Cruz Biotechnology	Cat#sc-1615; RRID: AB_630835
Rabbit polyclonal anti-Histone H3	Cell Signaling Technology	Cat#9715; RRID: AB_331563
Mouse monoclonal anti-GAPDH	EMD Millipore	Cat#MAB374; RRID: AB_2107445
Mouse monoclonal anti-FLAG M2-peroxidase (HRP)	Sigma-Aldrich	Cat#A8592; RRID: AB_439702
Mouse monoclonal anti-V5-peroxidase	Sigma-Aldrich	Cat#V2260; RRID: AB_261857
Mouse monoclonal anti-Myc-peroxidase	Sigma-Aldrich	Cat#11814150001
ANTI-FLAG M2 Affinity Gel	Sigma-Aldrich	Cat#A2220; RRID: AB_10063035
Pierce™ Anti-c-Myc agarose	Thermo Scientific	Cat#20168
GFP-Trap agarose	Chromotek	Cat#gta-20
succinylated Wheat Germ Agglutinin (sWGA) agarose	Vector Laboratories	Cat#AL-1023s; RRID: AB_2336863

(Continued on next page)

**Continued**

REAGENT or RESOURCE	SOURCE	IDENTIFIER
<b>Chemicals, Peptides, and Recombinant Proteins</b>		
LPS	Invivogen	Cat#tlrl-eblps
CpG	Invivogen	Cat#tlrl-1826
Pam3Cys	EMC	Cat#L2000
Nec-1	Enzo	Cat#BML-AP309
GSK-872	Calbiochem	Cat#530389
S3I-201	Sigma-Aldrich	Cat#SML0330
PUGNAc	Sigma-Aldrich	Cat#A7229
Cycloheximide	Sigma-Aldrich	Cat#C4859
zVAD	Calbiochem	Cat#627610
<sup>13</sup> C <sub>6</sub> -glucose	Sigma-Aldrich	Cat#A389374
<i>N</i> -acetylglucosamine	Sigma-Aldrich	Cat#A8625
OSMI-1	Aobious	Cat#AOB5700
GlcNAc	Sigma-Aldrich	Cat#A3286
IL-4	PeptoTech	Cat#214-14
ATP	Sigma-Aldrich	Cat#A7699
Nigericin	Invivogen	Cat#tlrl-nig
Silica	U.S. Silica	Cat#MIN-U-SIL 15
Aluminum	Thermo Scientific	Cat# 77161
CTB	Sigma-Aldrich	Cat#C9903
SYTOX Green Nucleic Acid Stain	Invitrogen	Cat# S7020
Hoechst 33342	Invitrogen	Cat# H3570
Recombinant murine IL-4	Peptotech	Cat#214-14
TRIsure	Bioline	Cat#BIO-38033
DMSO	Sigma	Cat#D2660
RPMI1640	Corning	Cat#10-040
Fetal Bovine Serum	Hyclone	Cat#SH30910.03
0.25% Trypsin	Corning	Cat#25-053
DMEM	Corning	Cat#10-013
X-tremeGENE HP DNA Transfection Reagent	Roche	Cat#06 366 236 001
FuGENE® 6 Transfection Reagent	Roche	Cat#11 814 443 001
M-MLV Reverse Transcriptase	Invitrogen	Cat#28025013
SuperSignal™ chemiluminescent HRP substrates	Thermo Fisher Scientific	Cat#34096
Power SYBR Green PCR Master Mix	Thermo Fisher Scientific	Cat#4367659
<b>Critical Commercial Assays</b>		
Mouse IL-6 ELISA Set	BD Biosciences	Cat#555240
Mouse TNF (Mono/Mono) ELISA Set	BD Biosciences	Cat#555268
Mouse IL-1β ELISA kit	Invitrogen	Cat#88701388
Mouse IL-2 ELISA kit	Invitrogen	Cat#88702488
Mouse IL-IFN <sub>γ</sub> ELISA kit	Invitrogen	Cat#88731488
Mouse IL-17A ELISA kit	Invitrogen	Cat# 88737188
Griess Reagent Kit	Invitrogen	Cat#G7921
Cytotoxicity Detection Kit (LDH)	Roche	Cat#11644793001
CellTiter-Glo® Luminescent Cell Viability Assay	Promega	Cat#G7570
Nuclear Extract Kit	Active Motif	Cat#40010
Phusion Site-Directed Mutagenesis Kit	Thermo Fisher Scientific	Cat#F541
<b>Experimental Models: Cell Lines</b>		
L929	ATCC	RRID: CVCL_0462
293T	ATCC	RRID: CVCL_0063

(Continued on next page)

**Continued**

REAGENT or RESOURCE	SOURCE	IDENTIFIER
THP-1	ATCC	RRID: CVCL_0006
OGT Knockout THP-1	manuscript in press	N/A
Experimental Models: Organisms/Strains		
Mouse: C57BL/6-LysM-Cre	The Jackson Laboratory	Strain#004781
Mouse: C57BL/6	The Jackson Laboratory	Strain#000664
Mouse: <i>Ogt</i> <sup>fl/fl</sup>	<a href="#">Shafi et al., 2000</a>	N/A
Mouse: <i>Ripk3</i> <sup>-/-</sup>	<a href="#">Newton et al., 2004</a>	N/A
Mouse: <i>Mik1</i> <sup>-/-</sup>	<a href="#">Murphy et al., 2013</a>	N/A
BMM: <i>Ripk1</i> <sup>K45A</sup>	<a href="#">Berger et al., 2014</a>	N/A
BMM: <i>Ripk3</i> <sup>K51A</sup>	<a href="#">Mandal et al., 2014</a>	N/A
Oligonucleotides		
OGT-targeted single gRNA	Manuscript in press	N/A
Primers for RT-PCR, see <a href="#">Table S4</a>	This paper	N/A
Primers for cloning, see <a href="#">Table S5</a>	This paper	N/A
Primers for mutagenesis PCR, see <a href="#">Table S6</a>	This paper	N/A
Recombinant DNA		
pCMV-HA-MyD88	Addgene	Addgene#12287
pcDNA3-HA-TRAF6	<a href="#">Yang et al., 2009</a>	N/A
pcDNA3-FLAG-RIPK1	Addgene	Addgene#78842
pCMV-FLAG-IKK1	Dr. Albert Baldwin	N/A
pCMV-FLAG-IKK2	Dr. Albert Baldwin	N/A
pcDNA3-FLAG-p65	<a href="#">Ashburner et al., 2001</a>	N/A
pcDNA3-NF-κB-Luc	<a href="#">Ashburner et al., 2001</a>	N/A
pWPXLd-OGT	Manuscript in press	N/A
pCMV-myc-OGT (WT)	<a href="#">Chen et al., 2013</a>	N/A
pCMV-myc-OGT (K908A)	Manuscript in press	N/A
pCMV-myc-OGT (H508A)	This paper	N/A
pCMV-myc-RIPK3	This paper	N/A
pCMV-myc-RIPK3-N	This paper	N/A
pCMV-myc-RIPK3-C	This paper	N/A
pcDNA3-FLAG-RIPK3	Addgene	Addgene#78815
pEGFP-N1-RIPK3 (human)	Addgene	Addgene#41387
pEGFP-N1-RIPK3 RHIM <sup>mut</sup>	Addgene	Addgene#41385
pEGFP-N1-RIPK3 (D160N)	Addgene	Addgene#41386
pEGFP-N1-RIPK3 (S199A)	Addgene	Addgene#41386
pEGFP-N1-RIPK3 (mouse)	Addgene	Addgene#41382
GIPZ Human RIPK3 shRNA	Open Biosystems	V2LHS_7679
pEGFP-N1-Caspase 8	<a href="#">Su et al., 2005</a>	N/A
pWPXLd	Addgene	Addgene#12258
pMD2.G	Addgene	Addgene#12259
psPAX2	Addgene	Addgene#2260
lentiCRISPR v2	Addgene	Addgene#52961
Software and Algorithms		
GraphPad Prism	GraphPad Software	GraphPad Prism, RRID: SCR_002798
I-TASSER program	<a href="#">Yang et al., 2015a</a>	I-TASSER, RRID: SCR_014627
PyMOL 2.1 software	PyMOL software	PyMOL, RRID: SCR_000305

## CONTACT FOR REAGENT AND RESOURCE SHARING

Further information and requests for resources and reagents should be directed to will be fulfilled by the Lead Contact, Haitao Wen ([haitao.wen@osumc.edu](mailto:haitao.wen@osumc.edu)).

## EXPERIMENTAL MODEL AND SUBJECT DETAILS

### Mice

*Ogt<sup>fl/fl</sup> × Lyz2-cre* mice were generated by crossing the *Ogt<sup>fl/fl</sup>* mice (Shafi et al., 2000) with lysosome M-Cre mice. C57BL/6 mice and lysosome M-Cre mice were purchased from Jackson Laboratories. *Ripk3<sup>-/-</sup>* (Newton et al., 2004) and *Mkl1<sup>-/-</sup>* (Murphy et al., 2013) mice have been previously described. *Ogt<sup>fl/fl</sup> × Lyz2-cre Ripk3<sup>-/-</sup>* and *Ogt<sup>fl/fl</sup> × Lyz2-cre Mkl1<sup>-/-</sup>* mice were generated by crossing *Ogt<sup>fl/fl</sup> × Lyz2-cre* mice with *Ripk3<sup>-/-</sup>* mice and *Mkl1<sup>-/-</sup>* mice, respectively. All mice were housed in SPF facilities at 21°C and 31% humidity. All mice were maintained under general housing environment and fed sterilized food (Chow TD. 7912; Harlan Teklad) and autoclaved water *ad libitum*. Mice were weaned at 28 days after birth, separated into same sex groups and all *in vivo* experiments were conducted in accordance with the guidelines established by the Ohio state University and the National Institute of Health Guide for the Care and Use of Laboratory Animals and the Institutional Animal Care and Use Committee (IACUC).

## METHOD DETAILS

### Reagents and antibodies

LPS and CpG were from Invivogen. Pam3Cys was from EMC Microcollections. Nec-1 was from Enzo. GSK-872 and zVAD were from Millipore. S3I-201, cycloheximide, PUGNAc, <sup>13</sup>C<sub>6</sub>-glucose and *N*-acetylglucosamine (GlcNAc) were from Sigma-Aldrich. Lipofectamine 2000 and the Griess Reagent Kit for nitrite quantification were from Thermo Fisher Scientific. Antibodies for immunoblotting included anti-OGT, anti-*O*-GlcNAc, anti-mouse p-RIPK1, anti-RIPK1, anti-p-IKK $\alpha/\beta$  (S176/180), anti-p-I $\kappa$ B $\alpha$  (S32), anti-I $\kappa$ B $\alpha$ , anti-p-p65 (S536), anti-p65, anti-p-ERK1/2 (T202/Y204), anti-ERK1/2, anti-p-JNK (T183/Y185), anti-p-p38 (T180/Y182), anti-p38, anti-p-STAT3, anti-STAT3, anti-Histone H3 (Cell Signaling Technology), anti-JNK1, anti-GFP, HRP-conjugated anti- $\beta$ -actin (Santa Cruz Biotechnology), HRP-conjugated anti-Flag (Sigma-Aldrich), HRP-conjugated anti-Myc (Roche), anti-IKK $\alpha$ , anti-NOS2, anti-GAPDH (Millipore), anti-RIPK3 (Novus Biologicals), anti-mouse MLKL (Abgent), anti-human p-RIPK3, anti-human p-MLKL, anti-mouse p-MLKL, anti-HMGB1 (Abcam), anti-IL-1 $\alpha$  (R&D Systems) and anti-mouse p-RIPK3 (Genentech). Antibody-conjugated agarose for immunoprecipitation included anti-Flag agarose (Sigma-Aldrich), anti-c-Myc agarose (Thermo Scientific), GFP-Trap agarose (Chromotek), and sWGA agarose (Vector Laboratories).

### Cell culture and stimulation

292T cells, L929 and THP-1 cells were purchased from ATCC and maintained under a humidified atmosphere of 5% CO<sub>2</sub> at 37°C in DMEM or RPMI 1640 supplemented with 10% fetal bovine serum (Sigma-Aldrich), respectively. To generate *RIPK3*-silenced THP-1 cells, GIPZ lentivector carrying shRNA targeting human *RIPK3* (V2LHS\_77679, Open Biosystems) were transfected into THP-1 cells. Infected cells were selected with 2  $\mu$ g/mL puromycin for 5 d. BMMs were generated from mice in the presence of L-929 conditional medium, as previously described (Li et al., 2017). Peritoneal macrophages were collected from peritoneal lavage with 10 mL sterile DPBS containing 2% FBS. Macrophages were stimulated with LPS (200 ng/mL), Pam3Cys (1  $\mu$ g/mL), CpG (2  $\mu$ g/mL), or LPS plus zVAD (10  $\mu$ M) for various periods as indicated in the Figure Legends. Cell culture supernatants were collected for ELISA or LDH release assay. Cells were collected for immunoblotting.

### RT-PCR

Total RNA was extracted from *in vitro* cultured cells using Trisure (Bioline). cDNA was synthesized with Moloney murine leukemia virus reverse transcriptase (Invitrogen) at 38°C for 60 min. RT-PCR was performed using SYBR Green PCR Master Mix (Applied Biosystems) in StepOnePlus detection system (Applied Biosystems). The fold difference in mRNA expression between treatment groups was determined by  $\Delta\Delta$ Ct method.  *$\beta$ -actin* was used as an internal control. The primer pair sequences of individual genes are listed in the Table S4.

### Immunoblotting

Electrophoresis of proteins was performed by using the NuPAGE system (Invitrogen) according to the manufacturer's protocol. Briefly, cultured BMMs were collected and lysed with RIPA buffer. Proteins were separated on a NuPAGE precast gel and were transferred onto nitrocellulose membranes (Bio-Rad). Appropriate primary antibodies and HRP-conjugated secondary antibodies were used and proteins were detected using the Enhanced Chemiluminescent (ECL) reagent (Thermo Scientific). The images were acquired with ChemiDoc MP System (Bio-Rad).

## ELISA

Cytokines in supernatant from *in vitro* cultured cells or cytokines in the peritoneal lavage fluids, serum or lung homogenates from animal experiments were quantified using the ELISA Set for mouse IL-6, IL-1 $\beta$  and TNF- $\alpha$  (BD Biosciences) according to the manufacturer's protocol.

## Nitrite quantitation

Nitrite generated from LPS-stimulated BMM were measured using the Griess Reagent Kit (Thermo Fisher Scientific) according to the manufacturer's protocol.

## Experimental sepsis animal models

For endotoxin shock model, mice were intraperitoneally administrated with LPS at 15 mg per kg body weight. CLP-induced polymicrobial peritonitis has been previously described (Wen et al., 2010). Briefly, mice were anesthetized with a combination of ketamine HCL and xylazine administrated intraperitoneally. A 1-cm midline incision was made to the ventral surface of the abdomen under sterile surgical conditions to expose the cecum. The cecum was partially ligated with a 3.0 silk suture at its base and punctured two times with a 21-G needle. Sham-operated mice underwent the identical operation except for the ligation and puncture. The cecum was returned to the abdomen cavity and closed with a surgical staple. Mice in both groups were treated with antibiotics intraperitoneally 6 and 24 hours after surgery.

## Plasmids and molecular cloning

pCMV vector expressing Myc-tagged human OGT has been described (Chen et al., 2013). FLAG-tagged RIPK3 (#78815), GFP-tagged RIPK3 (#41387), RIPK3 RHIM<sup>mut</sup> (#41385) and RIPK3 D160N (#41386) were purchased from Addgene. GFP-tagged RIPK3 S199A was kindly provided by Dr. Francis Chan (McQuade et al., 2013).

To generate the N- and C-terminal fragments of RIPK3, pcDNA3 vector expressing full-length RIPK3 was used as a template for PCR. To generate the lentivector expressing RIPK3, full-length RIPK3 WT or mutants were subcloned into the pWPXLd-EGFP lentivector (Addgene #12258). All primers used for cloning are listed in the Table S5. To generate a series of RIPK3 mutant constructs and OGT K908A, H508A mutant, Phusion Site-Directed mutagenesis Kit was used according to the manufacturer's instructions (Thermo Scientific). Primers for mutagenesis PCR are listed in the Table S6. All cloned genes were double-checked by sequencing.

## Cell transfection

As indicated in the Figure Legends, 293T cells were transfected for 30 h with a combination of expression plasmids for OGT WT, K908A or H508A mutant, and RIPK3 WT or mutants with X-tremeGENE HP DNA Transfection Reagent (Roche). For lentivector-based transduction, 293T cells were employed to package the pWPXLd lentivirus expressing RIPK3 WT or various mutants, which were further used to transduce *RIPK3*-silenced THP-1 cells.

## Luciferase assay

293T cells were transfected with NF- $\kappa$ B-driven luciferase reporter construct together with expression plasmids for MYD88, TRAF6, RIPK1, RIPK3, IKK1, IKK2 or p65, in the presence or absence of OGT using FuGENE6 (Roche). Empty pcDNA3 was used to maintain equal DNA amounts for transfection. Cells were harvested at 30 h post transfection. Luciferase units were measured as previously described (Lei et al., 2012).

## Metabolomics

$3 \times 10^6$  BMMs left untreated or stimulated with LPS for 4 h were harvested. The metabolite extraction was performed as previously described (Gunda et al., 2016). The media was aspirated, and the cells were washed twice with LC-MS grade water before lysing the cells. The metabolites were extracted using cold 80% methanol/water mixture and resuspended in 50% methanol/water mixture for further analysis using LC-MS/MS. A selected reaction monitoring (SRM) LC-MS/MS method with positive and negative ion polarity switching on a Xevo TQ-S mass spectrometer was used for analysis. Peak areas integrated using MassLynx 4.1 (Waters Inc.) were normalized to the respective protein concentrations. The resultant peak areas were subjected to relative quantification analyses with MetaboAnalyst 3.0. Further, principal component analysis, pathway impact analysis and heatmap were performed using MetaboAnalyst 3.0 software.

## Nuclear Magnetic Resonance (NMR) Spectroscopy analysis of <sup>13</sup>C-glucose metabolism

<sup>13</sup>C-labeling of UDP-GlcNAc from U-<sup>13</sup>C<sub>6</sub>-Glucose was detected from cell lysates using NMR spectroscopy-based metabolomics analysis. Briefly, samples were dried and then reconstituted using 550  $\mu$ L of 50 mM phosphate buffer in 100% D<sub>2</sub>O at pH 7.2 (uncorrected) with 500  $\mu$ M 3-(tetramethylsilane) propionic acid-2,2,3,3-d<sub>4</sub> (TMSF) as a chemical shift reference. 500  $\mu$ L of the supernatant was transferred to a 5 mm NMR tube for data acquisition. The NMR data were collected at 298K on an AVANCE III-HD 700 MHz spectrometer (Bruker) equipped with 5 mm quadruple resonance QCI-P cryoprobe (<sup>1</sup>H, <sup>13</sup>C, <sup>15</sup>N and <sup>31</sup>P) using ICON-NMR software (Bruker). A (2D) <sup>1</sup>H-<sup>13</sup>C heteronuclear single quantum coherence (HSQC) spectra was collected for each of the samples. The 2D <sup>1</sup>H-<sup>13</sup>C HSQC spectra were collected with 1K data points and a spectrum width of 11160 Hz in the direct dimension and 128 data points and a spectrum width of 29052 Hz in the indirect dimension. The 2D <sup>1</sup>H-<sup>13</sup>C HSQC spectra were processed with

NMRPipe (Delaglio et al., 1995). The spectra were Fourier-transformed, manually phased, zero-filled, apodized with a sine-bell window function, and baseline-corrected following solvent subtraction. All spectra were referenced to TMS<sup>p</sup> at 0 ppm. The processed spectra were then analyzed using NMRViewJ Version 8.0 (Johnson, 2018).

### **RIPK3 O-GlcNAcylation site mapping**

MS strategy was employed to identify RIPK3 O-GlcNAcylation sites, as described in our recent study (Li et al., 2017). Briefly, immunoprecipitated RIPK3 full length or C-terminal fragment from 293T cells was subjected to SDS-PAGE. The corresponding bands were excised and the proteins were reduced with DTT, alkylated with iodoacetamide, and digested with trypsin overnight, then subjected to LC-MS/MS analysis using a nanoAcquity (Waters Corp) coupled to an LTQ Orbitrap Velos (Thermo Scientific). The LTQ Orbitrap Velos was operated in data-dependent mode, and the 10 most intense precursors were selected for collision-induced dissociation (CID) fragmentation. Raw data files were processed using Proteome Discoverer (PD) version 2.0 (Thermo Scientific). Peak lists were analyzed using Sequest against a *Homo sapiens* Uniprot database. The following parameters were used to identify tryptic peptides for protein identification: 0.6 Da product ion mass tolerance; 10 ppm precursor ion mass tolerance; up to two missed trypsin cleavage sites; hexNAc (+203.0794 Da) of N/S/T; carbamidomethylation of Cys was set as a fixed modification; oxidation of M and phosphorylation of S/T/Y were set as variable modifications. The Percolator node was used to determine false discovery rates (FDR) and a peptide FDR of 5% were used to filter all results.

### **RIPK3 structure prediction**

The structure of human RIPK3 is predicted by the program I-TASSER (Yang et al., 2015a). The O-GlcNAcylation was added onto the predicted structure using PyMOL 2.1 software.

### **Statistics**

All experiments were performed a minimum of three independent replications. Statistical analysis was carried out with Prism 5.0 for Macintosh. All data are shown as mean  $\pm$  SD. The mean values for biochemical data from each group were compared by two-tailed Student's t test. Comparisons between multiple time points were analyzed by repeated-measurements analysis of variance (ANOVA) with Bonferroni post-tests. In all tests, *p* values of less than 0.05 were considered statistically significant.